ELSEVIER

Journal of Structural Geology 29 (2007) 1757–1780

JOURNAL OF STRUCTURAL GEOLOGY

www.elsevier.com/locate/jsg

Nucleation and initial growth of a shear zone network within compositionally and structurally heterogeneous granitoids under amphibolite facies conditions

Giorgio Pennacchioni [a,*], Neil S. Mancktelow [b]

[a] *Dipartimento di Geoscienze, University of Padova, I-35137 Padova, Italy*
[b] *Geologisches Institut, ETH Zürich, CH-8092 Zürich, Switzerland*

Received 26 February 2007; received in revised form 17 May 2007; accepted 18 June 2007
Available online 5 July 2007

Abstract

In the Neves area, the pre-Alpine intrusive protolith of the Zentralgneise unit (Tauern window, Eastern Alps) is well preserved in a kilometric-scale low-strain domain without pervasive Alpine deformation. It is compositionally heterogeneous, consisting predominantly of granodiorites, with lesser leucocratic granites, and different generations of lamprophyres and aplites. The intrusive rocks are crosscut by fractures that were locally infiltrated by fluids and surrounded by alteration haloes. Incipient Alpine amphibolite facies ductile deformation is strongly localized on these precursor fractures and on lithological planar heterogeneities, resulting in the development of several different types of shear zones. Fractures without alteration haloes initially accommodate slip entirely on the fracture itself. With increasing deformation, a foliation is progressively developed in the adjacent host rock, eventually producing a single heterogeneous ''ductile'' shear zone with the typical sigmoidal foliation pattern. Strong layers (aplite dykes and bleached alteration haloes developed to either side of precursor fractures) localize shear on their boundaries to produce characteristic paired shear zones. Shearing is more evenly distributed within weak layers (lamprophyres and quartz veins), with a marked discontinuity in shear strain against the adjacent, little deformed granodiorite. Shear zone development was accompanied by the formation of new fractures and quartz-rich veins in the host rock, which in turn also localized shear. Magmatic contacts, fractures and quartz veins are mostly steeply dipping and effectively span the complete range of strike orientations. The kinematics of the overprinting (strike-slip) shear zones was determined by the orientation of the initial discontinuities relative to the local principal compressive stress axis σ_1 (here oriented ca. 345°). Discontinuities of almost all orientations show shear reactivation, even in the case of very low resolved shear stress, indicating an overall viscous response of the system without a specific yield stress. The geometry and kinematics of the shear zone network suggest that the overall deformation in low-strain domains was close to coaxial. During deformation along the shear zone network, compatibility was maintained by fracturing (with the development of new quartz veins) and by distributed ductile deformation of the host rock, especially within contractional domains of the shear network and at shear zone intersections. Deformation never propagates into the undeformed homogeneous granodiorite as discrete ductile shear zones but is limited by the original extent of the precursor discontinuities. Shear zone development in intact rock is always preceded by fracturing, which localizes subsequent shear reactivation.
© 2007 Elsevier Ltd. All rights reserved.

Keywords: Shear zones; Quartz veins; Strain localization; Fractures

1. Introduction

Ductile shear zones (i.e. approximately tabular zones of localized shear strain within relatively undeformed host rock) are common deformation features in the middle to lower crust and upper mantle (e.g. Ramsay and Graham, 1970; Cobbold, 1977a,b; Carreras et al., 1980; Vissers et al., 1991). They are most clearly developed in rocks assumed to be effectively homogeneous and isotropic, such as large granitoid intrusions (e.g., Ramsay and Graham, 1970; Burg and Laurent, 1978; Ramsay and Allison, 1979), whereas layered or foliated rocks

* Corresponding author.
E-mail address: giorgio.pennacchioni@unipd.it (G. Pennacchioni).

0191-8141/$ - see front matter © 2007 Elsevier Ltd. All rights reserved.
doi:10.1016/j.jsg.2007.06.002

(e.g. sediments, schists and gneisses) are typically folded during subsequent deformation. Ductile shear zones in homogeneous isotropic materials are generally considered to develop due to rheology-dependent localization (e.g. Bowden, 1970; Cobbold, 1977b; Casey, 1980; Poirier, 1980), assumed to initiate at point-like flaws (Genter, 1993; Ildefonse and Mancktelow, 1993; Grujic and Mancktelow, 1998; Mancktelow, 2002, 2006; Mandal et al., 2004; Kaus and Podladchikov, 2006). Analytical, analogue and numerical models demonstrate that this localization is promoted by a combination of power-law viscous flow and strain softening behaviour (e.g. Bowden, 1970; Poirier, 1980; Mancktelow, 2002, 2006), potentially aided by softening due to shear heating (e.g. Brun and Cobbold, 1980; Kaus and Podladchikov, 2006). In these models, ductile shear zones develop without the need for any pre-existing planar discontinuities and some authors (e.g. Ingles et al., 1999) have indeed described ductile shear zones in granites that they inferred to have developed without the presence of any precursor.

Other authors, however, have argued that pre-existing brittle discontinuities play a major role in the nucleation of shear zones, as documented in several different granitoid bodies (Segall and Pollard, 1983; Segall and Simpson, 1986; Tullis et al., 1990; Guermani and Pennacchioni, 1998; Takagi et al., 2000; Mancktelow and Pennacchioni, 2005; Pennacchioni, 2005) and more recently even in strongly foliated schists (Fusseis et al., 2006). Such discrete precursor features may be obscured by subsequent ductile strain exploiting the same structures and can be overlooked. Shear zones in granitoids that exploit approximately planar lithological boundaries or layers of different composition have also been described (Christiansen and Pollard, 1997; Mancktelow and Pennacchioni, 2005; Pennacchioni, 2005). These compositional heterogeneities may be either primary (e.g. dykes) or secondary (e.g. related to fluid-rock interaction along brittle discontinuities) and may be stronger or weaker than the surrounding granitoid.

This paper describes the strong control of pre-existing brittle and compositional heterogeneities on the strain pattern developed within a granodioritic pluton under amphibolite facies metamorphic conditions typical of the middle to lower crust. The type of developing shear zone is determined by the competence of the precursor structure relative to the surrounding granodiorite, whereas the kinematics and amount of shear is determined by the orientation of the precursor structures with respect to the principal stress axes (i.e. by the geometric factor resolving the shear stress on a plane with a particular orientation). With the progressive development of a shear zone network, strain compatibility problems arise at the intersection of shear zones. In the case of rigid blocks, individual fault zones in conjugate systems must act in sequence (Ramsay and Huber, 1987, figures 23.16, 23.17). However, the interaction between crosscutting ductile shear zones has not been investigated in any detail. Here, we establish that the rigid block model cannot be extrapolated to ductile shear zones, which can act synchronously, with compatibility maintained by ductile flow within the intersection zone. Strain compatibility problems within the network of shear zones is not overcome by nucleation of new ductile shear zones in intact rock, but rather by the nucleation of new fractures, with subsequent exploitation of these fractures by ductile shear, or by the formation of domains of more diffuse heterogeneous strain and foliation development.

As emphasized in this paper, even large intrusive granitoid bodies, commonly taken as the best example of a relatively homogeneous and isotropic natural material, are in fact strongly heterogeneous in detail. Compositional and mechanical boundaries exert a controlling influence on the distribution, geometry and kinematics of the internal deformation structures within such a body, even if the strain on a larger scale may be relatively homogeneous. The deformation pattern cannot be understood without considering these pre-existing heterogeneities. Consistent with observations from other locations, it will be shown that shear zones always nucleate on precursor, approximately planar heterogeneities and never propagate as a localized shear structure into the host rock. The transition is always from brittle to ductile, even under amphibolite facies metamorphic conditions.

2. Geological outline

The area investigated in this study is located NE of the Neves lake (Lago di Neves or Nevessee, South Tyrol, Italy). Geologically it lies within the Tauern tectonic window, where Penninic units are exposed below Austroalpine units that otherwise dominate the Eastern Alps (e.g. Frisch et al., 1993). The lowermost and most extensive unit of the western Tauern window (Fig. 1) consists of pre-Alpine (ca. 310–290 Ma; Finger et al., 1993; Frisch et al., 1993) intrusive bodies of variable chemical composition, but largely dominated by granitoids (D'Amico, 1974), which were extensively converted to Alpine amphibolite facies orthogneisses and mylonites to form the "Zentralgneise" (e.g. Morteani, 1974). The Paleozoic schists and amphibolites intruded by these plutons, together with parautochthonous post-intrusive metasediments and amphibolites, are referred to in the literature as the "Lower Schieferhülle", whereas the overlying allochthonous Mesozoic calc-mica schists and ophiolitic units are referred to as the "Upper Schieferhülle" (e.g. Flügel and Faupl, 1987; Fig. 1). Peak pressures in the Lower Schieferhülle during the Alpine orogeny may have exceeded 1 GPa (Selverstone et al., 1984). However, in the Neves area, the subsequent thermal peak in metamorphism (known as the "Tauern metamorphism"; Hoernes and Friedrichsen, 1974; Friedrichsen and Morteani, 1979) occurred under amphibolite facies conditions estimated at 0.5–0.7 GPa and 550–600 °C (Fig. 1; Hoernes and Friedrichsen, 1974; Selverstone, 1985). The thermal peak of the Tauern metamorphism has been dated at ca. 30 Ma (Christensen et al., 1994), although temperatures may have remained high (within 20–30 °C of the maximum values) until ca. 20 Ma (von Blanckenburg et al., 1989; Christensen et al., 1994). This corresponds to the time when the western Tauern Window was rapidly exhumed in the footwall of the Brenner low-angle normal fault (Behrmann, 1988; Selverstone, 1988; Fügenschuh et al., 1997).

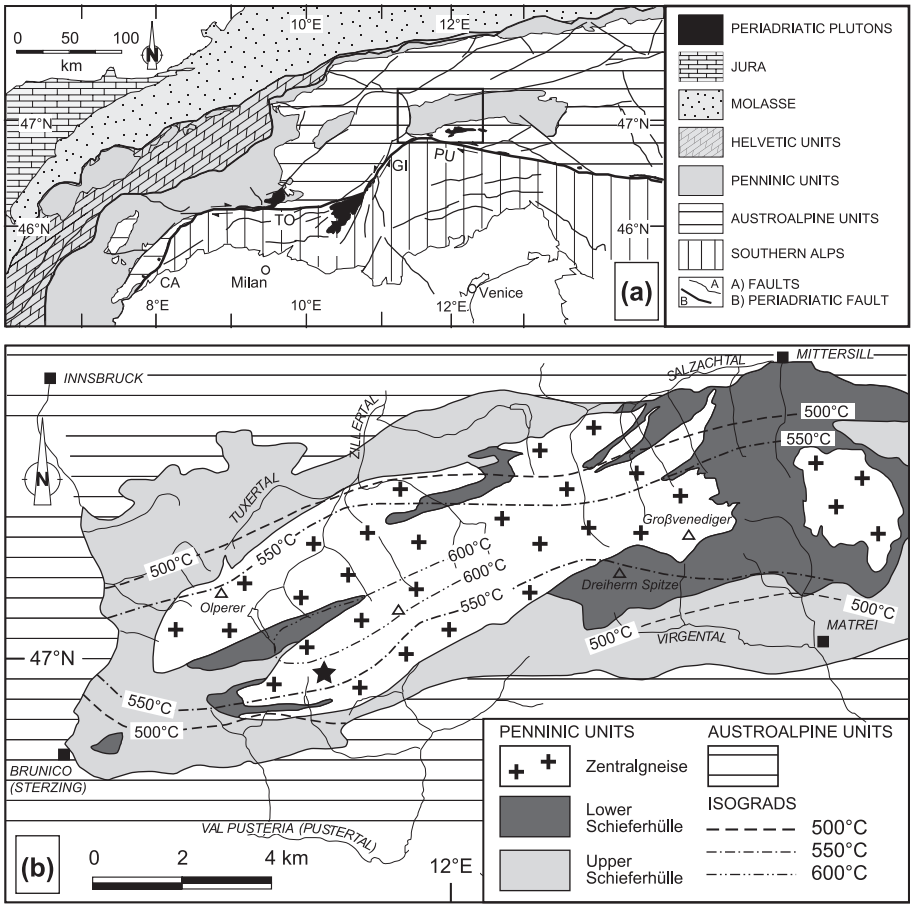

Fig. 1. Regional tectono-metamorphic setting of the Neves area. (a) Simplified tectonic map of the Alps, with inset marking the area of (b) at the western end of the Tauern Window. Local names of the main segments of the Periadriatic fault system are indicated: CA = Canavese; TO = Tonale; GI = Giudicarie; PU = Pusteria. (b) Simplified tectonic map of the western Tauern Window, with the location of the Neves area indicated by a star. Contours of peak temperatures attained in the Tauern Metamorphism are after Hoernes and Friedrichsen (1974).

The studied area represents a low-strain domain located just north of a kilometre-thick belt of granitoid mylonites that marks the south-eastern border of the Zillertal-Venediger Massif (Morteani, 1974; De Vecchi and Mezzacasa, 1986), which is the southernmost of the three main units of the Zentralgneise. This area has widespread, recently glaciated and perfectly polished outcrops at the base of the Mesule glacier, allowing very detailed and spatially continuous observation.

3. Pre-Alpine magmatic protolith

The pre-Alpine intrusive protolith is compositionally heterogeneous. The dominant and oldest unit is a medium-grained (millimetre grain size), rather equigranular granodiorite (quartz, plagioclase, biotite, ±K-feldspar, ±muscovite) with enclaves of more basic composition. SHRIMP U–Pb dating of zircons from a nearby outcrop of this granodiorite gave an age of 295 ± 3 Ma (Cesare et al., 2002). The intrusion generally preserves a magmatic foliation (mainly outlined by planar trains of biotite and by the marked elongation of basic enclaves) striking ca. N–S and steeply dipping. The granodiorites are locally intruded by finer-grained leucogranites, forming angular breccias (Fig. 2a), which are intimately associated with a first generation of mafic dykes (hereafter referred to as lamprophyre$_1$) showing spectacular magma mingling features with the granodiorites (Fig. 2a,b). These early mafic dykes are typically a few metres wide, strike ca. N to NNE and dip steeply. The granodiorites, granites and early basic dykes were intruded by different sets of aplitic dykes (Fig. 2a) that are variable in orientation, but most commonly strike E–W, and are also steeply dipping. The aplites are in turn crosscut by younger mafic dykes (lamprophyre$_2$) (Fig. 2c,d) also striking ca. E–W and steeply dipping, with a thickness in the range of few decimetres to several metres. The otherwise tabular shape of lamprophyre$_2$ locally shows step-like irregularities (Fig. 2c) occurring at regular intervals along strike, which developed at extensional linkage zones between magma-filled, en-echelon segmented fractures.

4. Structural precursors of Alpine ductile shear zones: fractures and veins

The pre-Alpine intrusives, including the aplite and lamprophyre dykes, are crosscut by steeply dipping discrete fractures (Fig. 3), which span a wide range of different orientations but with a strong predominance of ca. E–W strike directions. The

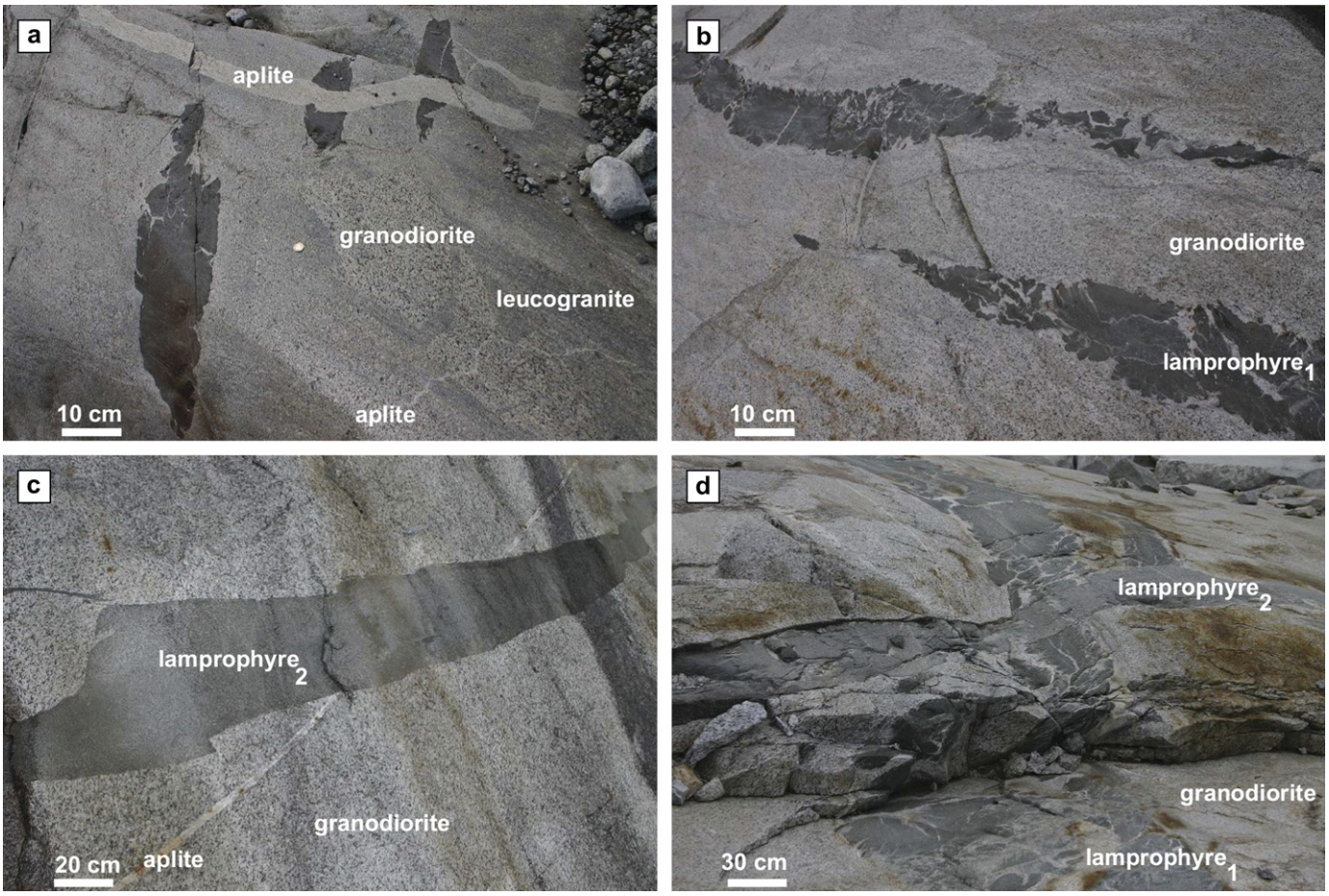

Fig. 2. Protolith magmatic structures. (a) Angular blocks of granodiorite within a leucogranite, which shows magma mingling relationships with isolated elongate blebs of a basic dyke (lamprophyre$_1$). All these rocks are subsequently cut by an aplite dyke. Looking W; GPS coordinates: N 46°58′25.5″, E 11°47′46.5″. (b) Magma mingling between a N–S-trending, segmented lamprophyre$_1$ dyke with an en-echelon geometry and the main granodiorite body. Looking E; GPS coordinates: N 46°58′31.1″, E 11°48′01.4″. (c) E–W-trending lamprophyre$_2$ crosscutting an aplitic dyke. Note the step-like irregularities in the dyke contact, due to coalescence of initial en-echelon magma-filled fractures. Looking N; GPS coordinates: N 46°58′33.9″, E 11°48′06.3″. (d) Intersection between a N–S-trending lamprophyre$_1$, showing magma mingling structures, and an E–W-trending, crosscutting lamprophyre$_2$. Looking SW; GPS coordinates: N 46°58′33.8″, E 11°48′02.9″.

fractures are very heterogeneously distributed, with some areas showing dense networks (Figs. 3a, 4) whereas other areas only have isolated fractures spaced on the 10 m scale. Fractures have a nearly straight trace in outcrop and are continuous over tens to hundreds of metres, although in detail they often consist of nearly coplanar sets of en-echelon segments with only slight overlap (Fig. 3a). The dominant E–W-striking fractures very typically (but not invariably) show a left-stepping pattern (Fig. 3a, Mancktelow and Pennacchioni, 2005, figure 5), as defined by Segall and Pollard (1980). Both analogue models (e.g. Riedel, 1929; Cloos, 1955; Morgenstern and Tchalenko, 1967; Tchalenko, 1970; Wilcox et al., 1973; Freund, 1974; Gamond, 1983, 1987; Richard et al., 1995) and field observations of shear zones and faults (e.g. Tchalenko and Ambraseys, 1970; Wilcox et al., 1973; Gamond, 1983, 1987) suggest that such a left-stepping pattern for primary fractures in an incipient shear zone is typical of an overall dextral sense of shear. However, other authors have described field relationships that clearly show the opposite sense, related to extensive pull-apart bridges between individual en-echelon fracture segments (e.g. Wilcox et al., 1973; Freund and Merzer, 1976; Aydin and Nur, 1982; Segall and Pollard, 1983). As discussed by Segall and Pollard (1980), both stepping senses are in fact observed in natural fault zones, and the offset cannot be used as an unequivocal shear sense criterion.

In the ‘‘undeformed’’ granodiorites, some fracture segments do not show any macroscopic offset of crosscut markers and single biotite grains can be matched across the fracture (i.e. the fractures are by definition ‘‘joints’’). These sealed joints can be easily missed, even on perfectly glacier-polished outcrops. However, they are often highlighted by discontinuous thin trails of biotite or by an alignment of rusty spots of alteration (probably related to the presence of pyrite grains scattered along the joint). Many joints are parallel to adjacent sheared fractures or show a transition to sheared fractures along their length. Initial shear reactivation of joints is very discrete and strongly localized on the fracture itself (Fig. 3b). In the absence of markers, the magnitude of this

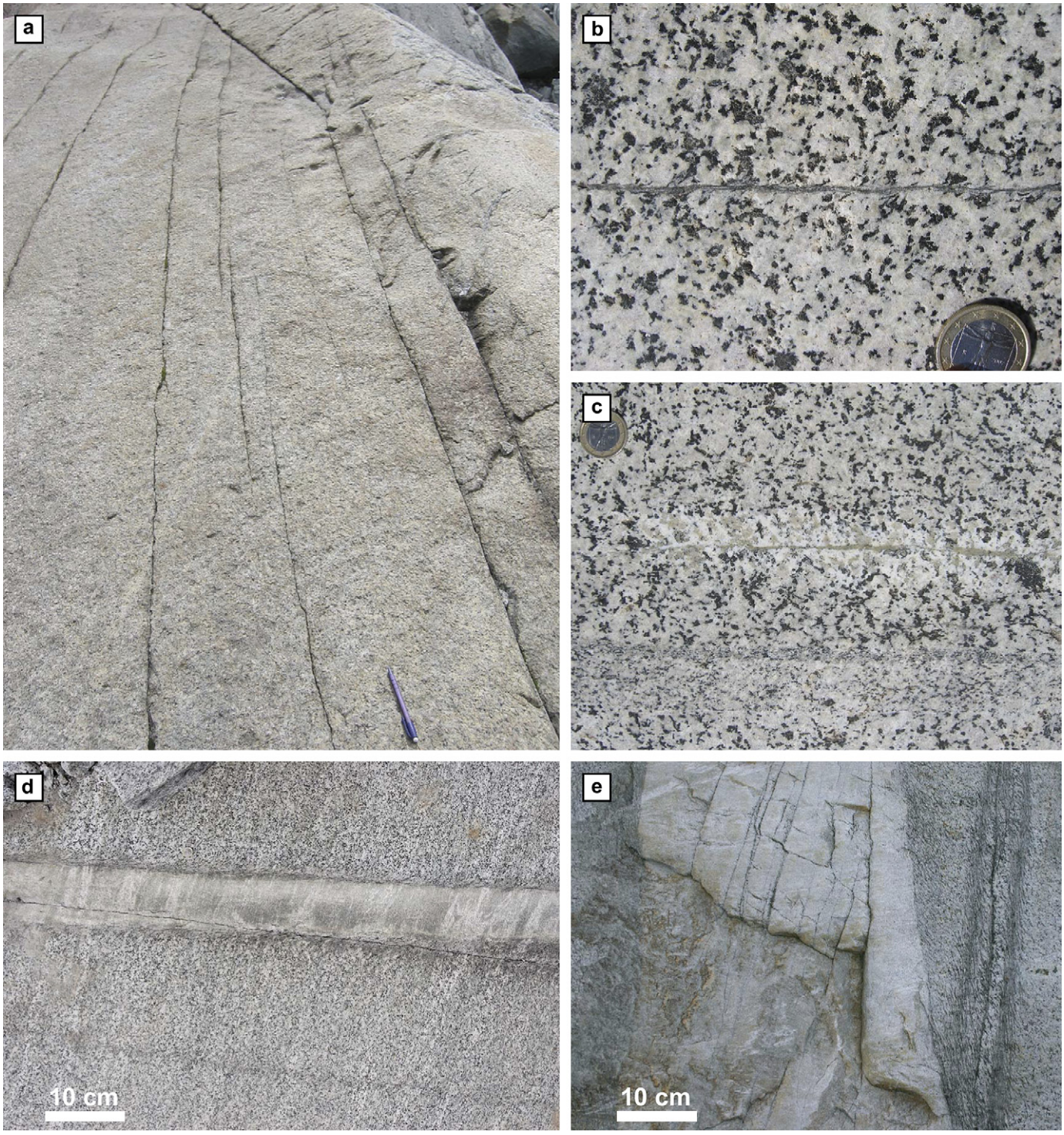

Fig. 3. Precursor fractures and alteration haloes. (a) Unreactivated precursor fractures showing the typical left-stepping geometry. Looking W; GPS coordinates: N 46°58′44.5″, E 11°48′29.4″; pen (14 cm long) for scale. (b) E–W-trending discrete fracture without an alteration halo. Dextral slip (ca. 10 cm from an offset thin aplite dyke ca. 20 cm to the left of the photo) is strongly localized on the fracture itself. Looking down, top to N; GPS coordinates: N 46°58′23.5″, E 11°47′47.5″; coin (2.3 cm in diameter) for scale. (c) Epidote-rich bleached halo without reactivation, as commonly developed on E–W-trending fractures. Looking down; top to N; GPS coordinates: N 46°58′25.1″ E 11°47′48.7″; coin (2.3 cm in diameter) for scale. (d) Aplite dyke transected at a low angle by a discrete fracture. Both the borders of the dyke and the fractures have been reactivated, with localized dextral shear. Looking down, top to N; GPS coordinates: N 46°58′28.3″ E 11°47′52.3″. (e) E–W-trending aplite dyke transected at a low angle by discrete fractures. The fracture in the granodiorite at the right, filled with biotite, has developed a bleached halo whose boundaries are reactivated, forming a paired dextral shear zone. Looking down, top to E; GPS coordinates: N 46°58′33.1″, E 11°48′03.2″.

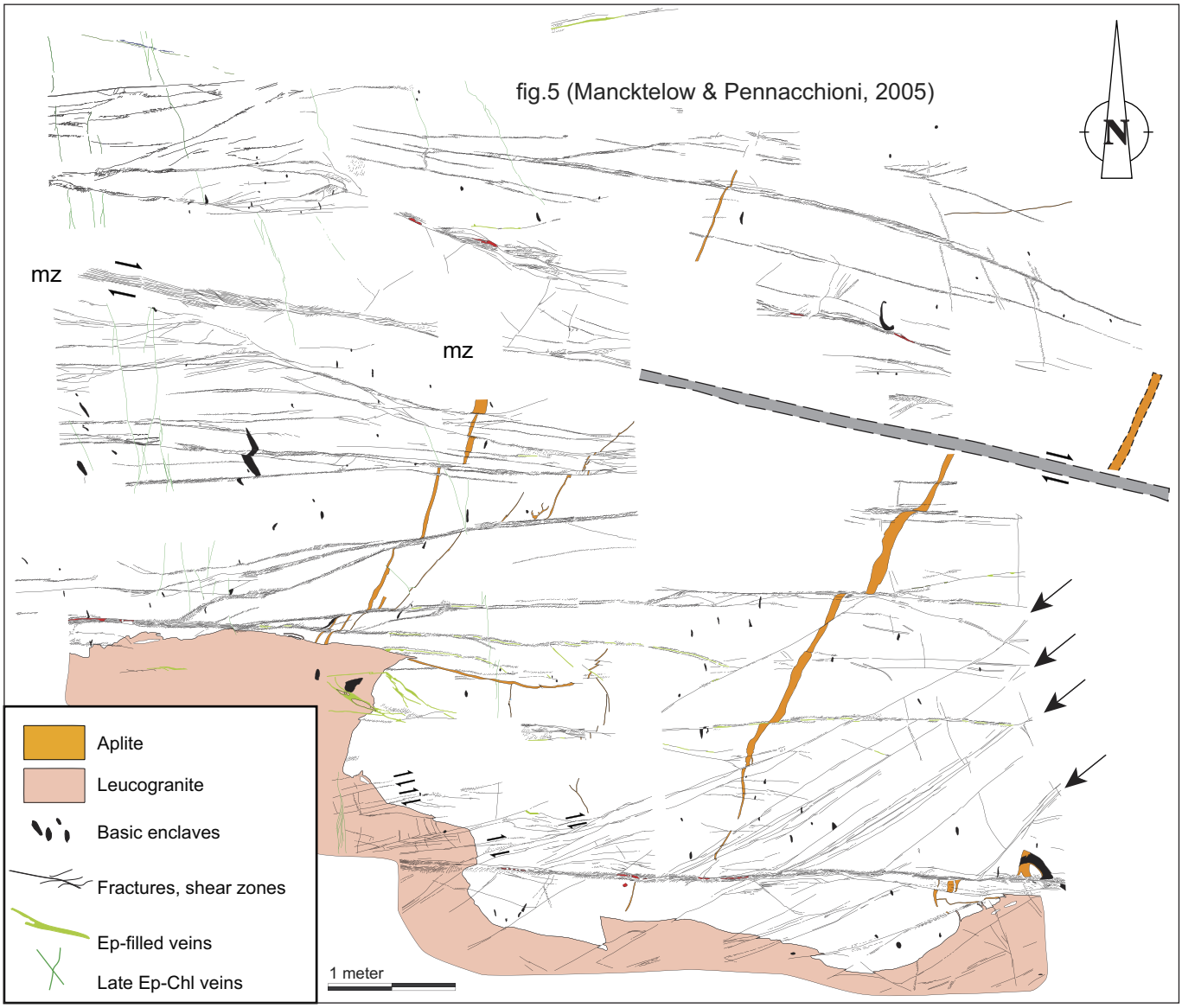

Fig. 4. Detailed surface map of a dense network of incipient shear zones. The large majority of shear zones in the outcrop are single or paired shear zones with an orientation scattered about E–W and a dextral sense of shear. The set of NNE-trending fractures that are well developed in the lower part of the outcrop (indicated by large black arrows) are specifically discussed in the text. The small double black arrows at the lower left side indicate a dextral reactivation of these fractures, which are mostly unreactivated elsewhere. There is one major mylonitic zone (labelled with "mz" and with an inferred continuation shown as the grey zone with dashed boundaries), accommodating an inferred offset of about 2 m (established from the offset of the aplite dyke), and a few other shear zones with significant offset in the outcrop. However, the great majority of shear zones only show offsets on the order of a few decimetres or less and have a thickness on the order of a few centimetres. The pattern of these minor shear zones generally still reflects the geometry of the precursor fractures, preserving original features such as Riedel and en-echelon arrangements or fracture splay geometries. An overview photo of the upper part of the outcrop, where the en-echelon segmentation is particularly clear, was published as figure 5c in Mancktelow and Pennacchioni (2005). Note the shape preferred elongation of the basic enclaves defining the magmatic foliation, with a ca. N–S to NNW–SSE strike. GPS coordinates (upper left corner of the map): N 46°58′23.2″, E 11°47′48.6″.

discrete offset is impossible to estimate (e.g., in the case of Fig. 3b, it is ca. 10 cm from the offset of an aplite dyke 20 cm to the left of the photo).

Many joints are filled with epidote (+quartz, +plagioclase, ±garnet), which forms millimetre-thick continuous veins or discontinuous patches. The vein-filled fracture segments are almost invariably surrounded by bleached haloes, generally less than 10 cm thick and symmetrically developed to either side of the vein (Fig. 3c). Other fractures are filled with biotite and show symmetric, coarse grained alteration haloes that can be more than 1 m thick, but are typically on the order of millimetres to centimetres. Veins and bleached/alteration haloes are most commonly observed along E–W joints but also occur on the N–S sets.

The age of jointing and associated veining is uncertain (see Section 9.1). Joints clearly post-date magmatic contacts and may crosscut these at small angles, without any tendency to

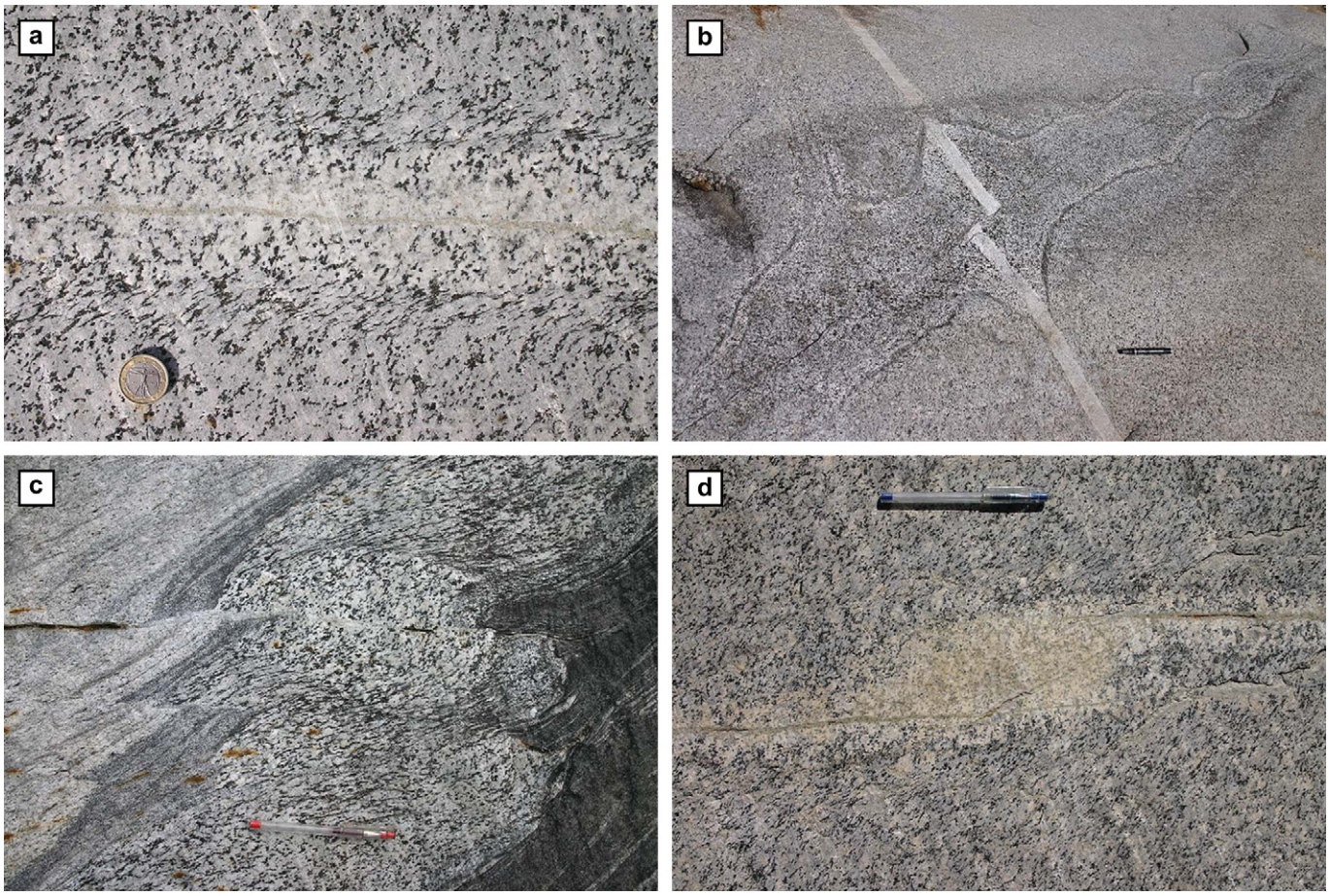

Fig. 5. Sense of shear on the central fracture. (a) Epidote-rich vein developed along an E–W-trending fracture, with a bleached halo developed symmetrically to either side. Dextral shear localization on the borders of the bleached zone produces a typical paired shear zone geometry. Looking down, top to N; GPS coordinates: N 46°58′37.0″, E 11°47′53.4″; coin (2.3 cm in diameter) for scale. (b) Alteration zone developed irregularly but symmetrically around an E–W-trending central fracture that has been reactivated in a dextral sense. The thin dark borders marking both boundaries between the altered and unaltered granodiorite are shear zones with the same dextral sense as the central fracture, but accommodating only very minor displacement. Looking NE; GPS coordinates: N 46°58′50.7″, E 11°47′37.8″; pen (13.5 cm long) for scale. (c) Paired shear zones with clearly sinistral offset on the central fracture/vein and opposite sense dextral reactivation at the borders of the altered zones. Looking down, top to S; GPS coordinates: N 46°58′36.7″, E 11°47′53.2″; pen (13 cm long) for scale. (d) Typical left-stepping, E–W-trending fractures, with epidote-rich alteration/bleaching and dextral shear localization at the borders, developing an incipient paired shear zone comparable to (a). Note, however, that the extensive alteration in the bridge zone and the bridging crack would be more typical of an extensional bridge, suggesting that initial shearing on the fracture may have been sinistral. Looking down, top to N; GPS coordinates: N 46°58′39.8″, E 11°47′56.6″; pen (13 cm long) for scale.

follow pre-existing compositional boundaries (Fig. 3d,e). Most joints are subsequently exploited by Alpine ductile structures, as discussed below.

5. Ductile deformation

5.1. Bulk strain

To a first approximation, the outcrops considered in this study can be taken to represent a low-strain domain consisting largely of ‘‘undeformed’’ intrusive protoliths. However, on closer investigation, a weak solid-state foliation (hereafter referred to as the ‘‘bulk foliation’’) is almost ubiquitous in the granodiorites. This foliation is subvertical and has a rather constant strike of around 075° throughout the whole area, i.e. nearly orthogonal to the magmatic foliation. It is macroscopically visible as a discontinuous foliation defined by fine lamellae of biotite transverse to the coarser, recrystallized magmatic biotite outlining the magmatic foliation. The magnitude of this background solid-state strain in the granodiorites is difficult to estimate precisely. The ellipticity of the basic enclaves is of little use as the enclaves were initially elongated, with variable aspect ratios (up to more than 5), due to magmatic flow. The principal shortening axis of the subsequent solid-state strain is close to the axis of maximum stretching for the magmatic fabric, so that enclaves initially decrease in ellipticity with tectonic strain and approximately equant enclaves can actually be indicative of a ‘‘significant’’ solid-state strain. This can be most clearly demonstrated where granodiorites are intruded by leucogranites. The later-stage leucogranites did not develop a magmatic foliation and the enclaves were initially equant. As a result, there is typically an abrupt change in the ellipticity and orientation of enclaves across the contact between

granodiorite and leucogranite, with the enclaves elongated ca. N–S and E–W respectively. This is because the ellipticity of the enclaves approximates the bulk strain ellipse in the leucogranite, whereas in the granodiorite it represents an overprint of the tectonic strain on a pre-existing elongate enclave shape developed due to magmatic flow.

5.2. Shear zones

The metagranitoids accommodate most strain on a network of different types of shear zones, which are invariably localized on approximately planar structural and compositional heterogeneities within the protolith. Quartz-rich veins that developed during the Alpine tectonic history (see Section 6 below) also acted as heterogeneities that localized shear during subsequent deformation. Most structural and compositional heterogeneities are steeply dipping and the shear zones that nucleate on them are also steep, with a stretching lineation that is near to horizontal. The flat polished outcrops at the front of the Mesule glacier therefore provide sections close to the XZ plane of maximum 2D strain.

The types of shear zones nucleating on fractures and on the alteration haloes surrounding mineralized (epidote, biotite) joints have been described in detail by Mancktelow and Pennacchioni (2005). In an early stage of ductile reactivation of joints, slip is accommodated along the original joint plane without any apparent deformation of the host granodiorite. These extremely localized knife-sharp shear zones (Fig. 3b) are macroscopically indistinguishable from unreactivated joints unless an offset marker is present (Mancktelow and Pennacchioni, 2005, figure 3b). A foliation is generally only developed at the contractional stepover between overlapping en-echelon terminations of these sheared joints, as has also been described in other granitoid massifs (Bürgmann and Pollard, 1992, 1994; Pennacchioni, 2005). With further slip, a foliation develops to either side of the sheared joints, extending for millimetres to a few

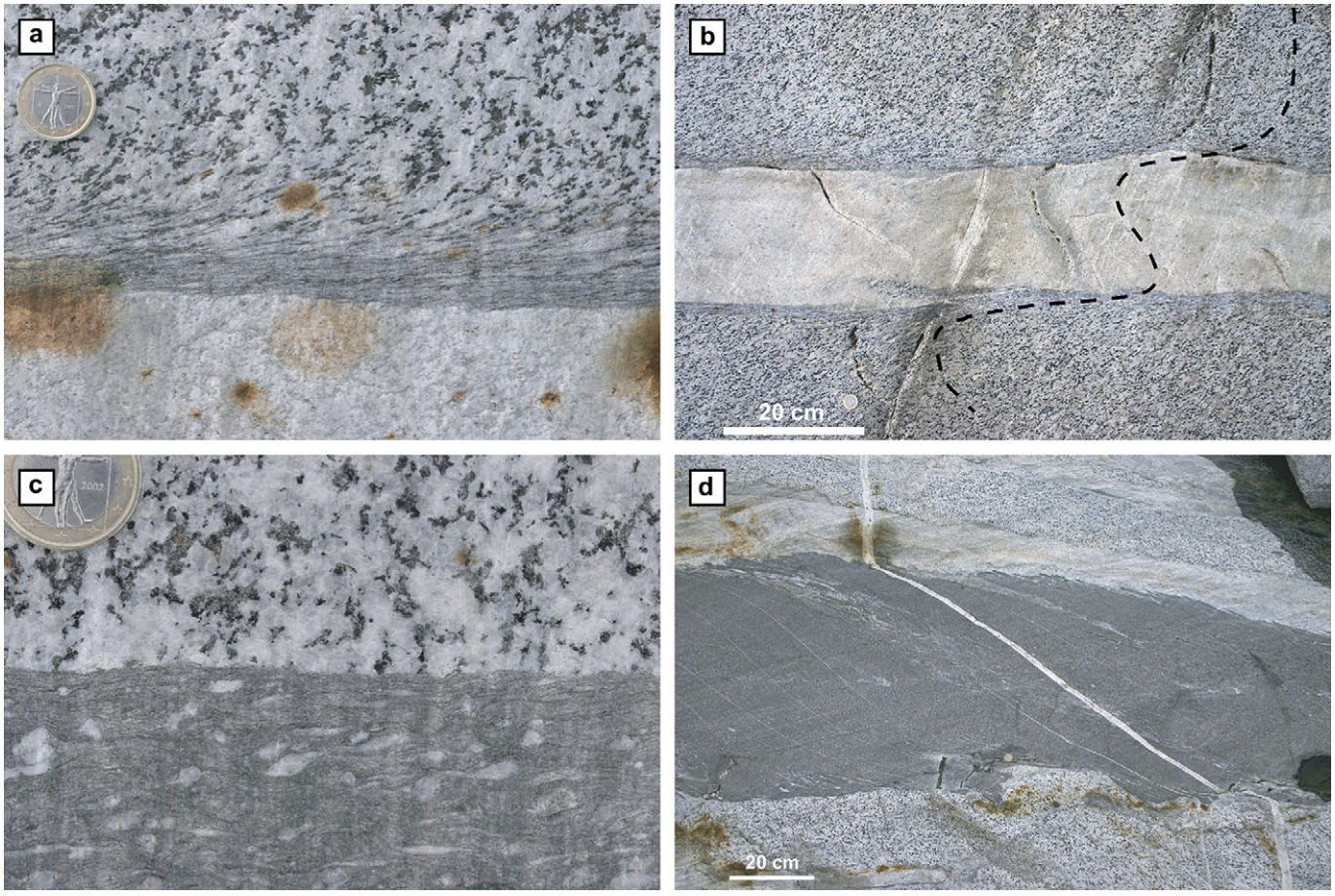

Fig. 6. Contrasting shear localization for strong (aplite) and weak (lamprophyre) dykes. (a) One side of a paired shear zone developed on an aplite dyke, with shearing concentrated on the aplite-granodiorite boundary and especially in the immediately adjacent host granodiorite. Looking down, top to N; GPS coordinates: N 46°58′28.9″, E 11°47′54.0″; coin (2.3 cm in diameter) for scale. (b) Synkinematic thin quartz-calcite vein acting as a marker and demonstrating the concentration of dextral shear strain at the border of an E–W aplite dyke. The dashed line outlining the trace of the vein has been drawn and moved to the right to highlight the relationships. Looking down, top to N; GPS coordinates: N 46°58′28.5″, E 11°47′46.5″. (c) Boundary between a lamprophyre dyke and the adjacent granodiorite, showing the very discrete jump from strong, relatively homogeneous strain in the lamprophyre to effectively no deformation in the granodiorite. Looking down, top to N; GPS coordinates: N 46°58′33.4″, E 11°47′54.8″; coin (2.3 cm in diameter) for scale. (d) Lamprophyre$_1$ showing a nearly homogeneous distribution of sinistral shear strain strongly concentrated within the dyke, as inferred from the crosscutting aplite. Looking down, top to W; GPS coordinates: N 46°58′36.5″, E 11°47′53.2″.

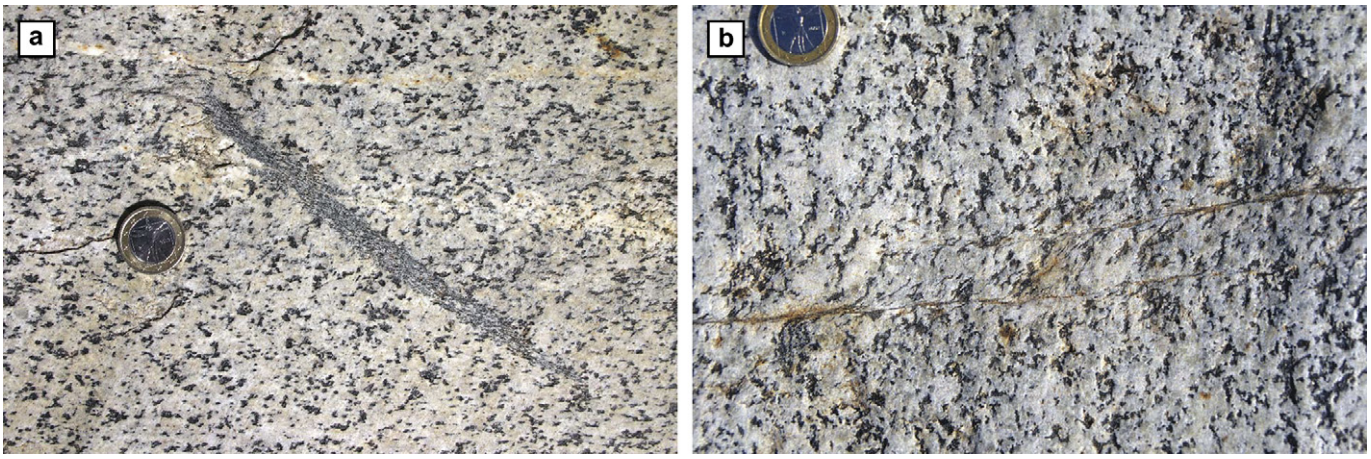

Fig. 7. (a) Localized shear of a basic enclave without propagation. The enclave shows a strong internal oblique foliation due to dextral shearing, but the shear zone has not propagated at the tip of the enclave as a discrete shear zone into the host granodiorite. Looking down, top to N; GPS coordinates: N 46°58′25.9″, E 11°47′50.0″; coin (2.3 cm in diameter) for scale. (b) Contractional bridge without propagation. Note that although the left-stepping precursor fractures have been reactivated in a dextral sense, forming a ductile contractional bridge, there is no evidence for propagation and linkage of the original fractures during subsequent reactivation. Looking down, top to N. GPS coordinates: N 46°58′28.60″, E 11°47′52.09″; coin (2.3 cm in diameter) for scale.

centimetres into the country rock. The foliation is initially straight but with increasing shear strain progressively develops a sigmoidal shape to form a ''classical'' ductile shear zone of a few centimetres thickness. The nucleation joint is often still visible in the centre of the shear zone. The spatial arrangement of these centimetre-thick shear zones perfectly mimics that of the original precursor joints, as is evident from the pattern of incipient shear zones in the map of Fig. 4,[1] with shear zones often arranged en echelon (Mancktelow and Pennacchioni, 2005, figure 5c). Closely spaced en-echelon arrangements of fractures on the centimetre to decimetre scale may result, as the result of ductile overprint, in structures resembling S−C′ mylonites (Berthé et al., 1979), with C′ planes corresponding to the initial joint segments.

Paired continuous shear zones are developed to either side of bleached alteration haloes surrounding mineralized joints (Fig. 5a; Mancktelow and Pennacchioni, 2005). In these paired shear zone systems, a discrete and sometimes quite significant offset (up to the metre-scale) is commonly observed across the central vein or joint (Fig. 5b). This is especially typical of biotite-filled joints (Mancktelow and Pennacchioni, 2005, figure 7). Where discernible, the offset on the central fracture is generally the same as the sense of the flanking paired shear zones, which is dextral for the dominant E−W-trending set (Fig. 5b). This would be consistent with an interpretation of the typical left-stepping arrangement of these precursor fractures in terms of dextral shear (e.g. Gamond, 1987). However, in a minority of cases, the offset along E−W-trending central veins is sinistral and therefore opposite to the dextral sense of shear generally observed for flanking paired shear zones with this orientation (Fig. 5c). Epidote-rich alteration and bleaching zones preferentially developed at some left-stepping bridges between EW fractures also suggest an initial sinistral reactivation (Fig. 5d).

The bleached halo between paired shear zones usually appears very little deformed (Fig. 5a,b) and may survive as a slightly deformed band within broader mylonites (e.g. Mancktelow and Pennacchioni, 2005, figure 6f). Where epidote-rich alteration and bleaching is discontinuously present along a joint, paired shear zones develop around the altered parts and merge to a single shear zone along the unaltered segments. Variation in thickness of the bleached zone can in some cases be quite marked over short distances but is always quasi-symmetric about the central vein (Fig. 5b). Shear localization only occurs on the boundaries of the altered zone and shear zones overprinted by bleaching haloes have not been observed.

Aplite dykes commonly develop paired shear zones due to shear localization at their boundaries (Fig. 6a; Mancktelow and Pennacchioni, 2005, figure 8). The strain distribution within the aplites is macroscopically difficult to determine because of the absence of biotite and the fine grain size of white mica outlining the foliation within the aplite (Fig. 6a). However, in some cases quartz-calcite veins developed during shearing crosscut the aplite dykes and provide initially near planar markers that are deformed during paired shear zone formation (Fig. 6b). These markers confirm that deformation is concentrated on the aplite boundaries and particularly in the immediately adjacent granodiorite, with a less deformed (to undeformed) zone in the core of the aplite dyke.

In contrast to the aplites, lamprophyres typically show (1) strong localization of deformation internally within the dyke, with very little or no involvement of the adjacent granodiorite

[1] The map shown in Fig. 4, as well as the maps of Figs. 9, 12 and 14, were drawn from high-resolution photomosaics. Photos were taken in the field with the use of a 1 m square aluminium grid marked off in 10 cm units that was moved to cover the complete area of interest. For each grid, two partially overlapping 6-megapixel photos were taken. Photo pairs of the grid were then orthorectified to eliminate photo distortion using ER-mapper software, and merged to a single photo. Merged photos were assembled into a photomosaic that was georeferenced using the coordinates of corners of each grid determined by differential GPS. This procedure allowed a precision in mapping on the order of 1−2 cm. The high-resolution maps are available as supplementary material.

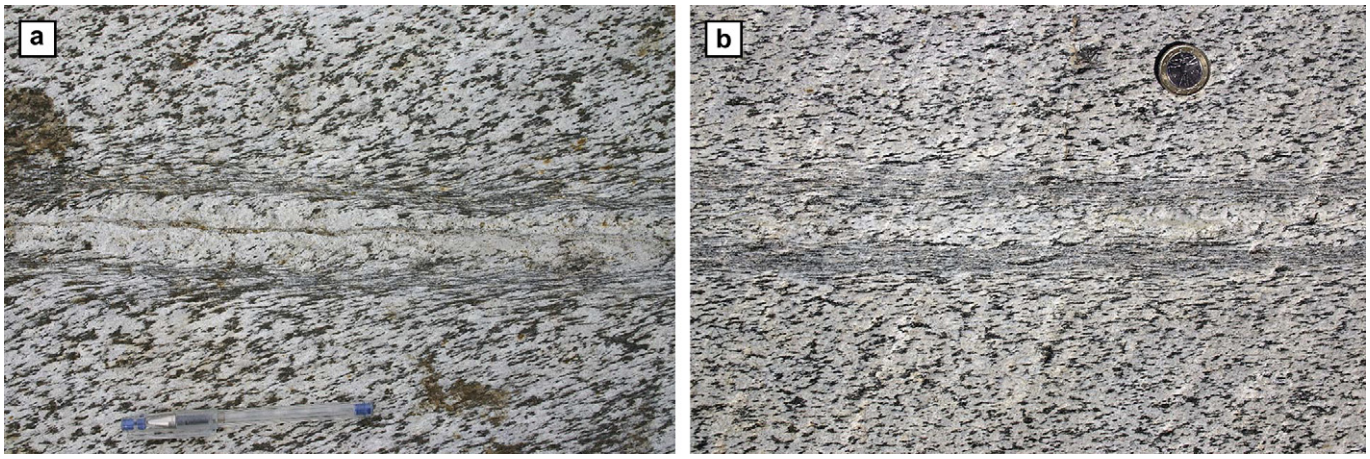

Fig. 8. (a) Typical monoclinic dextral paired shear zone. Looking down, top to N; GPS coordinates: N 46°58′52.0″ E 11°48′14.4″; pen (13 cm long) for scale. (b) Symmetric paired shear zone showing enhanced foliation development subparallel to the bleached zone boundaries. Looking down, top to NNW; GPS coordinates: N 46°58′21.0″ E 11°47′59.0″ (WP132-pag122); coin (2.3 cm in diameter) for scale.

(Fig. 6c), and (2) a nearly homogeneous distribution of shear strain, without localization toward the boundaries (Fig. 6d). Strain localization at the lamprophyre boundary has only been observed in some of the thickest dykes, probably reflecting the original presence of chilled margins with different rheological properties.

Shear zones can be directly linked either to pre-existing joints or dykes, or to synkinematically developing veins, and are limited by the length and orientation of these precursor structures. Single aplite dykes can be quite variable in orientation within a single outcrop, but shear zone localization invariably follows the boundaries and does not diverge into the host granodiorite. In fact, the variation in dyke orientation can lead to a change in the sense of reactivation along a single shear zone, with necessary accommodation problems, but the shear zone still follows the pre-existing boundary rather than propagating into the host granodiorite. In the map of Fig. 4, the set of NNE-trending fractures that are well developed in the lower part of the outcrop (and indicated by black arrows) are either not reactivated or only slightly sheared. However, where the shear sense is discernible, it consistently changes from sinistral for the bottom-right examples to dextral for the top-left examples. This inversion in shear sense reflects the slight change in orientation of the fractures, in a clockwise sense, moving from bottom-right to top-left. It demonstrates that only very small differences in orientation are sufficient to change the shear sense and, implicitly, that shear reactivation occurs for only very small components of resolved shear stress.

Shear zones do not extend beyond the length of the original precursor structure. In Fig. 7a, for example, localized shearing is developed in a basic enclave but does not extend into the surrounding granodiorite beyond the tip of the enclave. The lack of in-plane propagation typically results in a very strong displacement gradient toward the end of shear zones. Precursor fractures are also apparently not capable of in-plane propagation during reactivation, as indicated by the lack of linkage or convergence of discrete fractures in contractional bridges (Fig. 7b). A similar observation was made in a granodiorite pluton from the central Sierra Nevada (California) by Segall and Pollard (1983), who noted that fractures (joints) reactivated as faults ‘‘did not propagate into intact rock in their own planes as shear fractures’’.

In the large majority of cases, the different types of shear zones have a clear monoclinic asymmetry indicative of the sense of shear (Fig. 8a). There are, however, zones that develop a foliation parallel to the precursor structural or compositional heterogeneity and to the bulk foliation of the host rock (Fig. 8b). These symmetric zones are developed adjacent to alteration zones that were oriented approximately perpendicular to the local shortening direction (see Section 7).

5.3. Strain accommodation in the shear zone network: intersection zones and diffuse deformation

Shear zones of different orientation and sense of shear are often present in the same outcrop and may intersect each other. Fig. 9 is a detailed outcrop map illustrating the complex architecture of such a shear zone network. Compatibility problems must arise for non-parallel and intersecting shear zones if all structures are active at the same time. As seen in Figs. 9b and 10, mutual overprint of shear zones can produce strong thinning of associated quartz veins and dykes in the intersection zone. A marked foliation is generally present in these zones, which gradually fades away from the intersection region (Fig. 10d). In many cases, the amount of mutual offset of the shear zones at the intersection is comparable and both the foliation and the thinning zones are subparallel to the regional bulk foliation in the granodiorite (Fig. 10c,d). In other cases, one of the shear zones dominates and shows only a relatively minor offset in the intersection zone (Fig. 10a,b).

Compatibility is also maintained by more diffuse deformation of the host granitoid, as recorded by gradients in intensity of the bulk foliation on the outcrop scale. For example, the bulk foliation is especially evident on the contractional sides of shear zone and quartz vein tips, with the decrease in

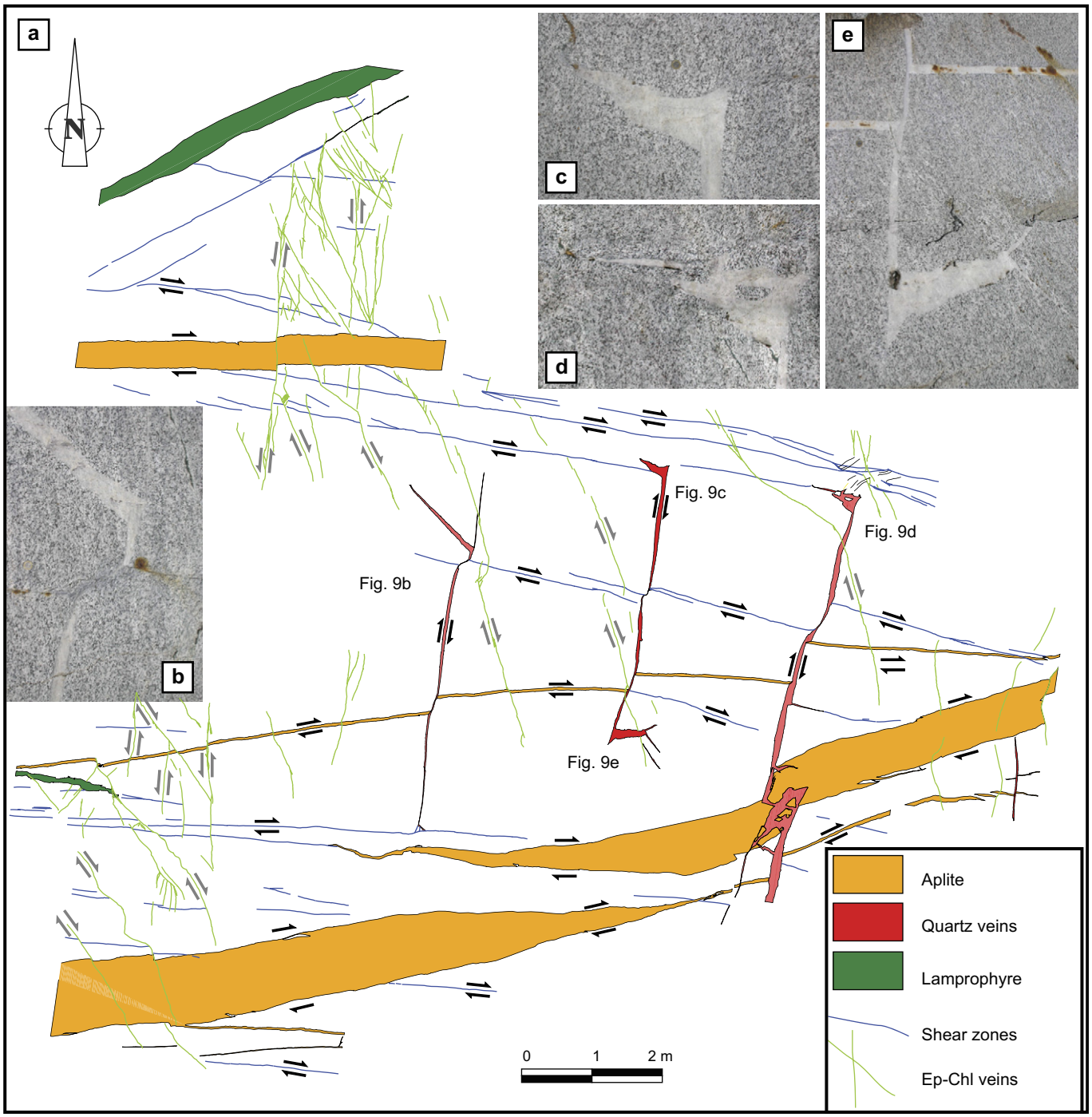

Fig. 9. Detailed surface map showing a set of subparallel double-winged sinistral quartz veins associated with dextral shear zones and exploiting differently oriented precursor fractures and aplite dykes. The double arrows indicate the sense of shear of amphibolite facies shear zones (black arrows) and of late-stage chlorite-epidote filled faults (grey arrows). The photo of inset (b) is an enlargement of the intersection between a quartz vein with a wing geometry indicating opening under sinistral shear and a dextrally reactivated fracture, with the development of a typical thinned and strongly foliated zone at the intersection. The inset photos (c), (d) and (e) are enlargements of the wings developed at the quartz vein tips. GPS coordinates: N 46°58′33.8″, E 11°47′55.4″.

displacement toward the tip of these zones being accommodated by more distributed strain in the adjacent matrix.

6. Synkinematic fracturing: quartz-rich veins

Veins consisting of quartz (dominant in most veins), calcite (Fig. 11a,b), biotite (Fig. 11c) and plagioclase are common in the Neves area (Cesare et al., 2001). They range in size from a few millimetres to a few metres in width and up to several tens of metres in length, but most of the veins do not exceed a few metres length and a few decimetres thickness (Figs. 9, 11, 12). The veins are quite variable in their 3D shape. The simplest are approximately tabular to lens-shaped over most of their length. More complex vein shapes show (1) wings

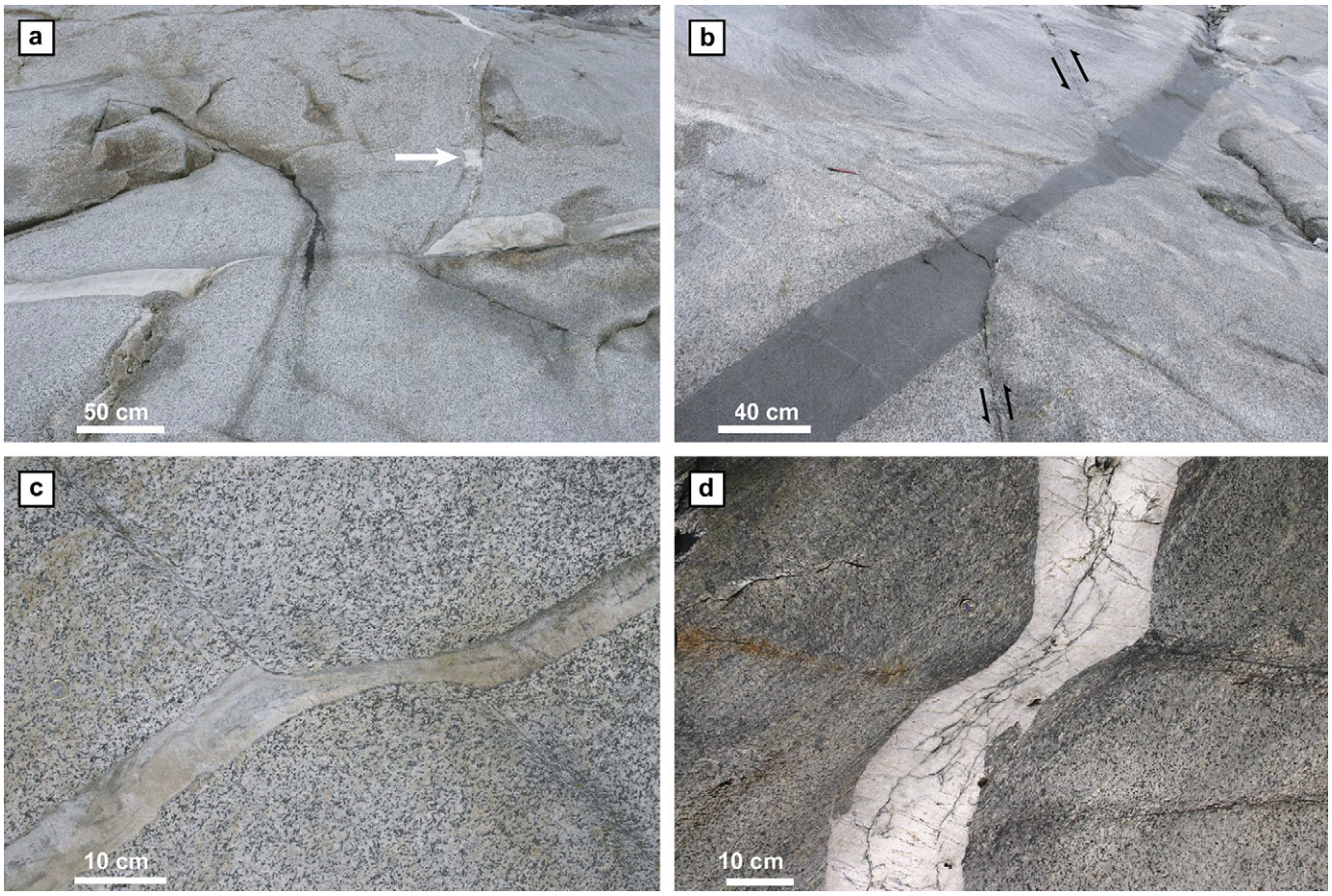

Fig. 10. Thinned intersection zones. (a) Asymmetric thinned zone at the intersection between an E–W aplite dyke, with a dextral paired shear zone developed at its boundaries (which dominates the overall structure), and a ca. N–S quartz vein. The sense of shear along the vein is sinistral, as indicated by the small asymmetric pull-apart indicated by the arrow. A strong localized foliation is developed in the granodiorite within the intersection zone, with an asymmetry consistent with the dominant dextral shearing. Looking N; GPS coordinates: N 46°58′28.5″, E 11°47′46.5″. (b) Asymmetric thinning of a dextrally sheared lamprophyre$_2$ dyke at the intersection with a sinistral shear zone exploiting a fracture. Looking NE. GPS coordinates N 46°58′28.5″, E 11°47′46.5″. (c) Symmetric thinned zone at the intersection between a quartz vein (sinistral) and a sheared fracture (dextral). The mutual offset on the two shear zones is approximately the same magnitude and consequently there is no shear component along the thinning zone. Looking down, top to NW; GPS coordinates: N 46°58′28.6″, E 11°47′51.8″. (d) Nearly symmetric thinned zone at the intersection between a sinistrally sheared quartz vein and a dextrally sheared fracture. A strong foliation has developed in the host granodiorite close to and parallel to the thinned zone. Looking down, top to N; GPS coordinates: N 46°58′23.1″, E 11°47′47.6″.

Fig. 11. Quartz veins features. (a) Undeformed quartz-calcite vein within the granodiorite. The weak oblique shape fabric to the coarse calcite grains is consistent with a sinistral sense of shear during opening of the vein. Looking down, top to E; GPS coordinates: N 46°58′35.1″, E 11°47′55.3″. (b) Pull-apart geometry of a quartz-calcite vein indicating a sinistral sense of shear during vein opening. The boundary foliation developed in the granodiorite to either side of the vein, just to the right of the pull-apart and along the upper boundary with the granodiorite, consistently indicates sinistral shear during ductile overprint. Looking down, top to E; GPS coordinates: N 46°58′26.0″, E 11°46′49.4″. (c) Quartz-biotite vein with an internal foliation oblique to the vein boundary, indicating relatively homogeneous sinistral shear within the vein. Note that the host granodiorite is effectively undeformed. Looking down, top to E; GPS coordinates: N46°58′28.5″, E 11°47′52.1″; coin (2.3 cm in diameter) for scale. (d) E–W sheared joint that displaces a thin aplite dyke (boundaries highlighted by white lines) dextrally by 8 cm and is in turn crosscut and offset sinistrally by a quartz-calcite vein. Looking N. GPS coordinates: N 46°58′26.0″, E 11°47′45.3″. (e) Horn-shaped wings at the opposite tips of a quartz vein, indicating sinistral sense of shear during vein opening. Some spikes that diverge from the main vein body and are subparallel to the wing tips are also visible on the upper side of the vein (indicated by arrows); these spikes most likely record different pulses of vein propagation. Looking down, top to E; GPS coordinates: N 46°58′33.6″, E 11°48′05.8″. (f) Quartz vein crosscutting a mylonite zone within the granodiorite. Looking down, top to E; GPS coordinates: N 46°58′49.5″, E 11°48′10.3″. (g) Multiple generations of quartz-calcite veins. The veins labelled 1 to 3 have developed in sequence during ductile deformation, with the older ones showing more clockwise rotation (due to the dextral shear) than the younger ones. The veins are dragged into the paired shear zone flanking the aplitic dyke (most clear here on the upper dyke boundary) and the sequential development of the veins is also reflected in the decreasing amount of displacement from vein 1 to vein 3. Inside the aplite, each vein has an orientation similar to that in the granodiorite outside the shear zone, demonstrating that shear strain was concentrated at the aplite-granodiorite boundary (as was also illustrated in Fig. 6b). Within the aplite, dashed lines have been drawn (and moved slightly to the right) to highlight the trace of the veins. Looking down, top to N; GPS Coordinates N 46°58′28.5″, E 11°47′46.5″. (h) N–S-trending quartz vein showing a protrusion into an adjacent alteration halo, developed around an E–W fracture. The dashed black line delineates the contact between the vein and the bleached granodiorite. The shape of the quartz vein protrusion is clearly inherited from the shape of the altered zone. Looking down, top to N; GPS coordinates: N 46°58′29.9″, E 11°48′04.3″.

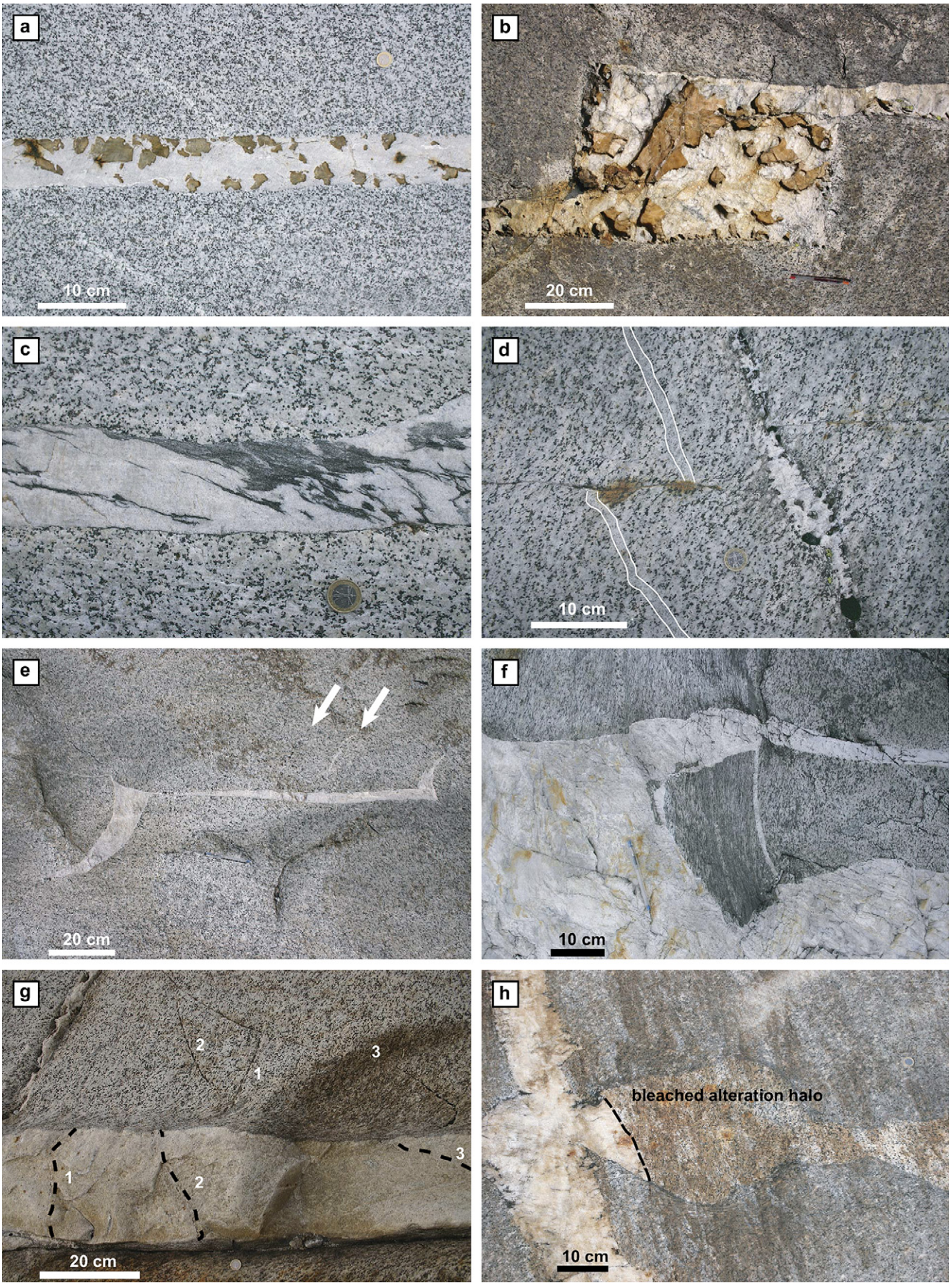
a
10 cm
b
20 cm
c
d
10 cm
e
20 cm
f
10 cm
g
1
2
3
1
2
3
20 cm
h
bleached alteration halo
10 cm

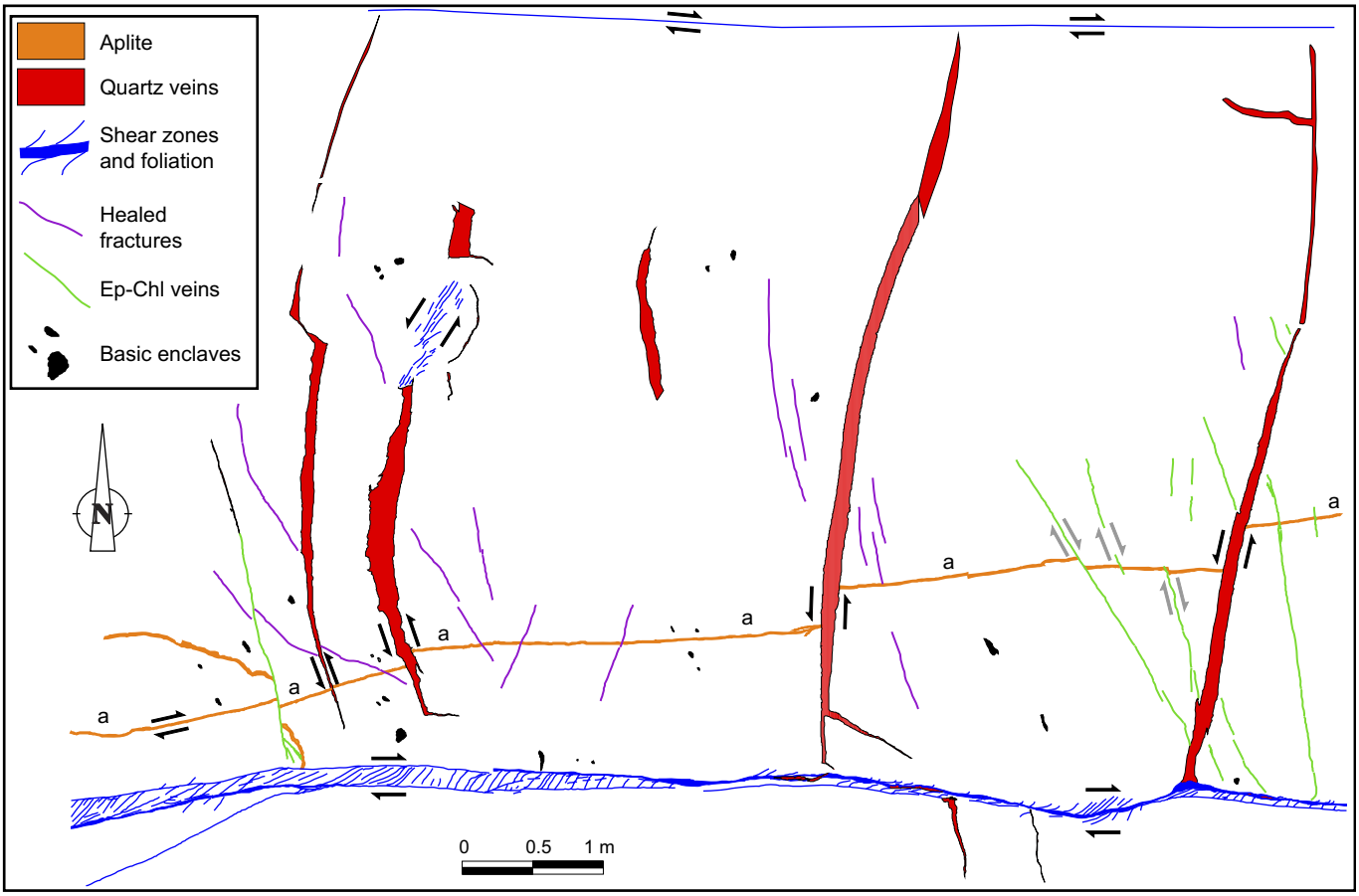

Fig. 12. Detailed outcrop map of a typical set of sub-parallel quartz veins at a high angle to the bounding E–W shear zones, which developed from precursor fractures. The veins accommodated sinistral shear both during opening and ductile reactivation, as indicated by the wing geometry of some veins, the offset of a thin aplite dyke (labelled with "a") crosscut by the veins, and the asymmetry of foliation in the granodiorite developed at a contractional jog at the tip of one vein. Later fractures filled with epidote–chlorite veins have a more NNW to NW strike and a dominant dextral sense of shear. GPS coordinates: N 46°58′23.8″, E 11°47′48.6″.

developed on one or both vein tips, in the latter case always on opposite sides (Figs. 9, 11e; e.g. Willemse and Pollard, 1998), (2) pull-apart structures (Fig. 11b), (3) stepped boundaries, reflecting an initial en-echelon arrangement of fractures, and (4) spikes or branches, subparallel to the wings, but diverging from the main vein at locations away from the tips (Fig. 11e). Wings taper away from the parent vein and may be straight (pennant-shaped wings, Fig. 9) or, more commonly, curved (horn-shaped wings) (Fig. 11e). The tips of horn-shaped wings usually have an orientation nearly orthogonal to the bulk foliation of the host granodiorite. Quartz veins are typically relatively "short" structures when compared to the joints and epidote-rich veins decorating these joints (Section 4), which can be traced along strike for (many) tens of metres.

The veins can occur in isolation or in arrays of sub-parallel structures (e.g. Figs. 9, 12), spaced on the order of one to a few metres but never forming dense networks. Veins are present throughout the whole range of strain domains, from apparently little deformed areas to strongly mylonitic zones. In low strain domains, the veins commonly flank, or are confined between, major shear zones (Fig. 12). Mostly the veins do not crosscut the shear zones themselves (e.g. Fig. 12) but this is not invariably the case (Fig. 11f). Veins in the granodiorite are commonly arrested or blunted directly at the contact to lamprophyre dykes. They are sometimes associated with a cuspate-lobate bending of the lamprophyre contact, suggestive of a boudinage-like instability of the granodiorite against the less competent lamprophyre (Fig. 13). Blunt terminations of quartz veins are not observed against fractures or discrete sheared fractures, but are sometimes present against thick shear zones. In some cases, subparallel veins occur with a roughly regular spacing beside shear zones (Fig. 12). In some sheared lamprophyre$_2$ dykes, veins are specifically located at steps in the contact that are related to the original en-echelon arrangement of dyke segments (Fig. 14). Some veins cut straight through sheared joints and clearly do not exploit pre-existing fractures (Fig. 11d).

Most veins have been overprinted by ductile deformation. In low strain domains, quartz-rich veins tend to localize ductile deformation. Within the veins themselves, however, strain is relatively homogeneous, with the development of a straight foliation inclined to the vein boundaries (Fig. 11c). This

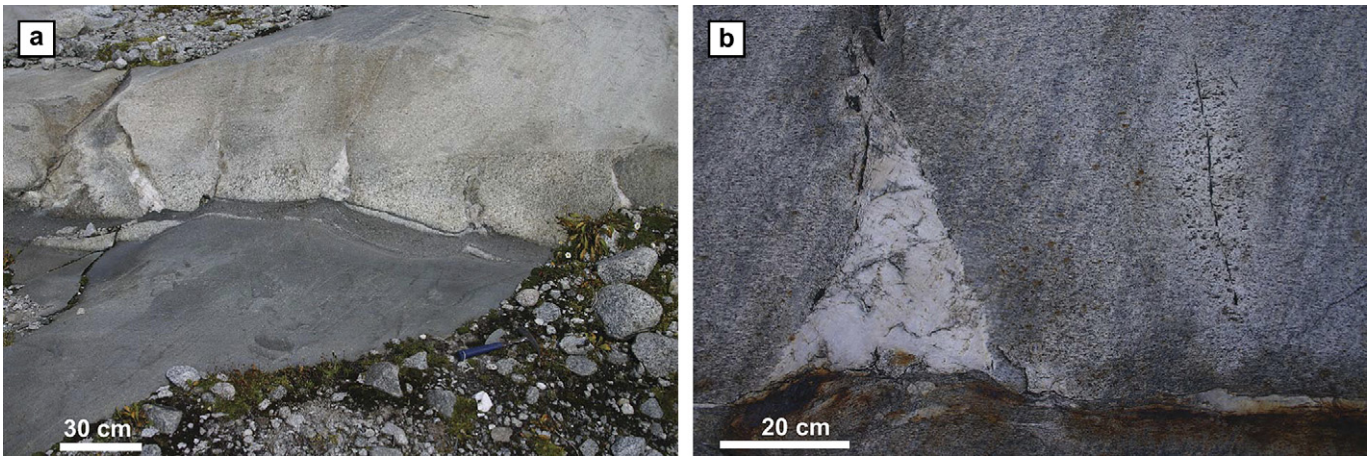

Fig. 13. (a) Incipient boudinage of a granodiorite–lamprophyre$_2$ boundary, with the spacing and orientation of coeval quartz veins controlled by this mechanical instability. Looking N. GPS coordinates: N 46°58′25.4″; E 11°47′47.8″. (b) Triangular quartz vein developed in granodiorite at the boundary with a lamprophyre$_2$ dyke. Note, on the right side of the quartz vein, the thin chlorite-filled fracture surrounded by a bleached alteration halo, which has also developed, at a later stage, orthogonal to the compositional boundary. Looking down, top to N.

geometry is similar to that typically observed in the lamprophyres, but distinctly different to that for the aplites, where strain is strongly partitioned to the dyke boundaries. As a result of shearing along the veins, a more strongly foliated domain is commonly present in the host rock on the contractional side of the vein tips, on the opposite side to the wings. The asymmetry of the geometric elements (e.g. wings, pull aparts or rhomb openings) of veins nearly invariably indicates the same sense of shear during opening as indicated by the solid state fabric during ductile deformation (Fig. 11b). For example, veins with left-stepping wings or pull-aparts also show sinistral ductile fabrics. A total of 394 quartz veins were investigated of which (1) 129 (33%) did not show any recognizable ductile fabric, marker offset or geometric shape asymmetry useful to establish the sense of shear, (2) 231 (59%) show a sinistral sense of shear, and (3) only 34 (9%) are dextral. Only five veins showed a contradiction in the interpreted sense of shear for opening and ductile shearing.

In broad shear zones, quartz veins occur both as undeformed veins cutting the mylonitic foliation at a high angle (Fig. 11f) and as mylonitic quartz veins transposed into the foliation, suggesting that vein development has been multi-stage. In the weakly deformed rock, crosscutting relationships between quartz veins are rare. However, this has been observed for thin quartz-calcite veins at the boundary of paired shear zones flanking an aplite dyke (Fig. 11g: same location as Fig. 6b). In this example, younger veins crosscut different generations of older veins that have undergone different amounts of clockwise rotation under dextral shear within the paired shear zones flanking the aplite dyke.

Quartz veins crosscut epidote-filled joints, but the opposite overprinting relationship has never been observed. In

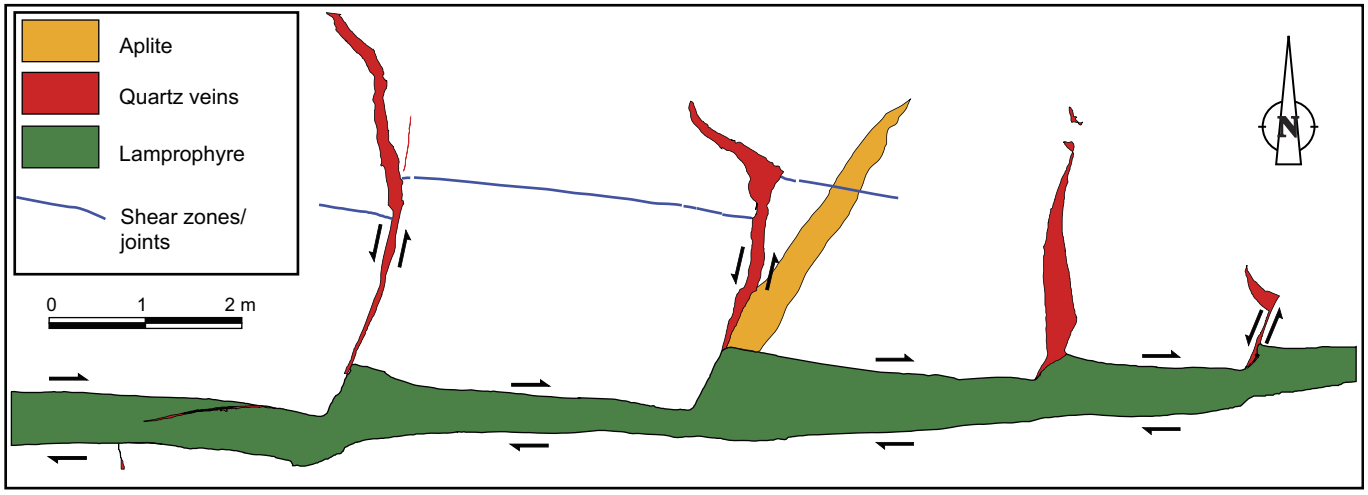

Fig. 14. Detailed outcrop map of the control of original steps in the lamprophyre$_2$ dyke boundary on quartz vein formation. GPS coordinates: N 46°58′32.2″, 11°48′02.8″.

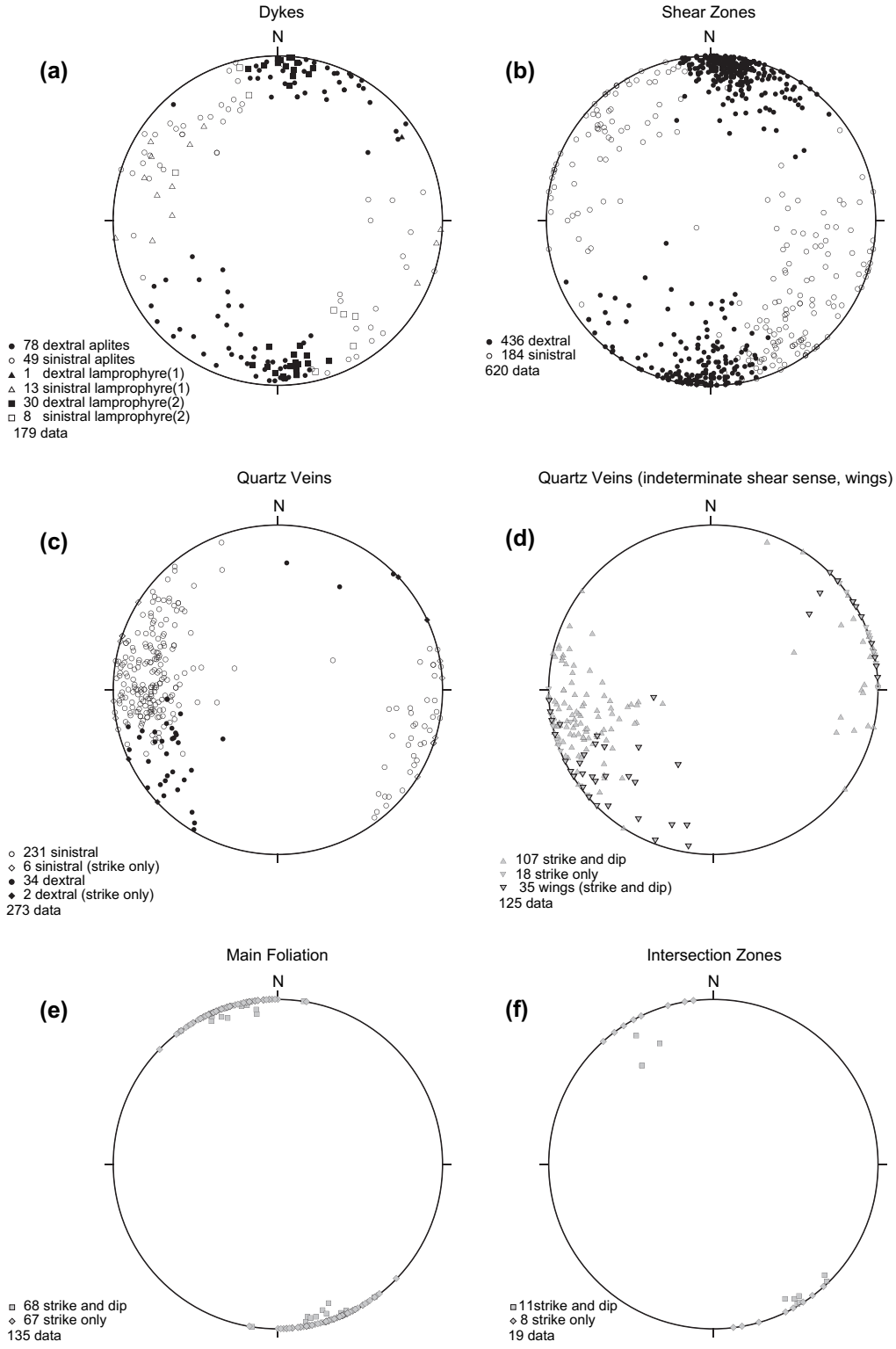

Fig. 15. Orientation data for pre-Alpine intrusive protolith and Alpine amphibolite facies structures, plotted in stereographic projection (lower hemisphere).

Fig. 11h, the quartz vein has clearly partly followed the pre-existing bleached zone at the intersection between the quartz vein and the paired shear zone, which developed around the bleaching halo to either side of the central fracture. The quartz vein protrusion is mimetic and preserves a ghost structure of the bleaching halo. Such overprinting relationships indicate that the quartz veins developed during a later stage, after formation of the joint and the associated fluid-rock interaction that produced the bleaching halo along the joint.

7. Orientation and shear zone kinematics

The orientations of the different compositional and structural elements, together with the kinematics of the associated Alpine shear zones, are summarized in the stereoplots of Fig. 15. Most structures are steeply dipping. Lamprophyre$_1$ dykes mainly strike N–S to NE–SW and localize sinistral ductile shear, whereas lamprophyre$_2$ dykes strike E–W and show a dextral shear reactivation (Fig. 15a). Aplite dykes span a quite wide range of orientations, with a consistent pattern of either dextral or sinistral boundary reactivation dependent on their orientation (Fig. 15a). E–W-striking dykes with dextral kinematics are the most common (51% of the aplite dykes show dextral reactivation, 32% sinistral, and 17% no reactivation) (Fig. 15a). In some cases, a transition from dextral to none to sinistral reactivation can be observed as the orientation varies along the same aplite dyke. Single and paired shear zones that exploited joints and mineralized joints surrounded by bleached haloes show a strong maximum in strike orientation around E–W and dominantly dextral kinematics (ca. 75% of these shear zones) (Fig. 15b). The large majority of quartz veins are scattered around a N–S strike and show opening features and ductile fabrics consistent with a sinistral sense of shear (59% of these veins are sinistral, 9% dextral and, for the rest, the sense of shear could not be determined) (Fig. 15c). Of the 34 dextral veins observed, 6 were clearly intruded along a pre-existing aplite dyke. It is important to note that veins for which the sense of shear could not be determined (i.e. they do not show any clear macroscopic asymmetry, marker offset or ductile fabric) have a clear preferred orientation with a maximum 344°/74°E (strike/dip) (Fig. 15d), which is exactly orthogonal to the bulk foliation in the granodiorite (Fig. 15e). The tips of quartz vein wing structures (e.g. Figs. 9, 11e) show a similar maximum in strike around NNW.

Taken as a whole, the structural and compositional discontinuities span the complete range of strike directions and the kinematics of shear zones localized on these discontinuities are very consistent. It should be emphasized that practically all orientations of pre-existing heterogeneities have been utilized as zones of localized ductile shear, although the amount of this shear is variable and difficult to quantify. What can generally be established is the sense of shear and this defines two quadrants, one sinistral and one dextral. As shown in the cumulative plot of Fig. 16, there is an abrupt switch from a dextral to a sinistral sense of shear at strike directions of ca. 345° and 75°. The 345° direction also corresponds to (1) the mean pole of the bulk foliation in the granodiorite (Fig. 15e), (2) the maximum in strike orientation of quartz veins without a discernible shear component during or subsequent to opening (Fig. 15d), and (3) the maximum in strike of wing crack tips measured from the quartz veins (Fig. 15d). This implies that the principal axes of stress (reflected in crack and vein formation) and finite strain (reflected in the bulk foliation) were effectively coaxial in the generally low strain areas where these measurements were collected.

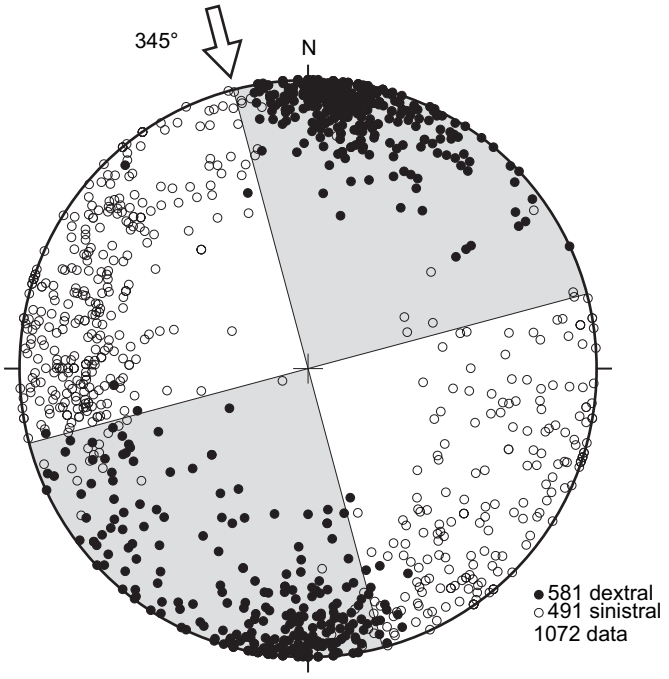

Fig. 16. Cumulative plot of orientation data (stereographic projection, lower hemisphere). The grey and white sectors in the plot represent the orientation ranges of planar pre-existing structures or compositional boundaries that have been exploited as dextral or sinistral shear zones, respectively. Overall, these data indicate that the principal compressive stress direction was 345°.

8. Late-stage fractures and veins

The amphibolite facies ductile fabric is overprinted by a set of conjugate shear and extensional fractures filled with epidote, chlorite, quartz and zeolite (Figs. 4, 9, 17). These fractures and veins are typically a few millimetres to, in the case of the extensional fractures, a few centimetres in thickness. The conjugate sets may be isolated or arranged in brittle damage zones, a few decimetres to a few metres wide, confined between pairs of bounding master faults subparallel to one of the conjugate fault sets (Fig. 9). These brittle fault zones are discontinuous along strike (Figs. 4, 9) and often have an en-echelon geometry on the scale of several metres (Fig. 4). The angle between conjugate shear fractures sets is significantly less than 60° and typically in the range 25–35° (Figs. 4, 9, 17b). This suggests mixed-mode fracturing under relatively low effective confining pressure (i.e. in the parabolic region of the Mohr-Coulomb failure envelope).

One large sinistral fault zone transects the area studied, with an orientation of ca. 015–020°/70° W (strike/dip) and an offset of ca.10 m. The orientation, general microstructure and mineralogy of this sinistral fault are identical to that of the major Giudicarie Fault occurring 60 km to the SW, near Merano (Fig. 1a). The Giudicarie Fault has an offset of 15–20 km (Viola et al., 2001) and pseudotachylyte developed along the Passeier Valley segment of this fault has been dated at 17.3 ± 1.1 Ma by Müller et al. (2001).

The orientation pattern of dextral and sinistral late-stage faults and extensional veins is quite consistent (Fig. 18) and

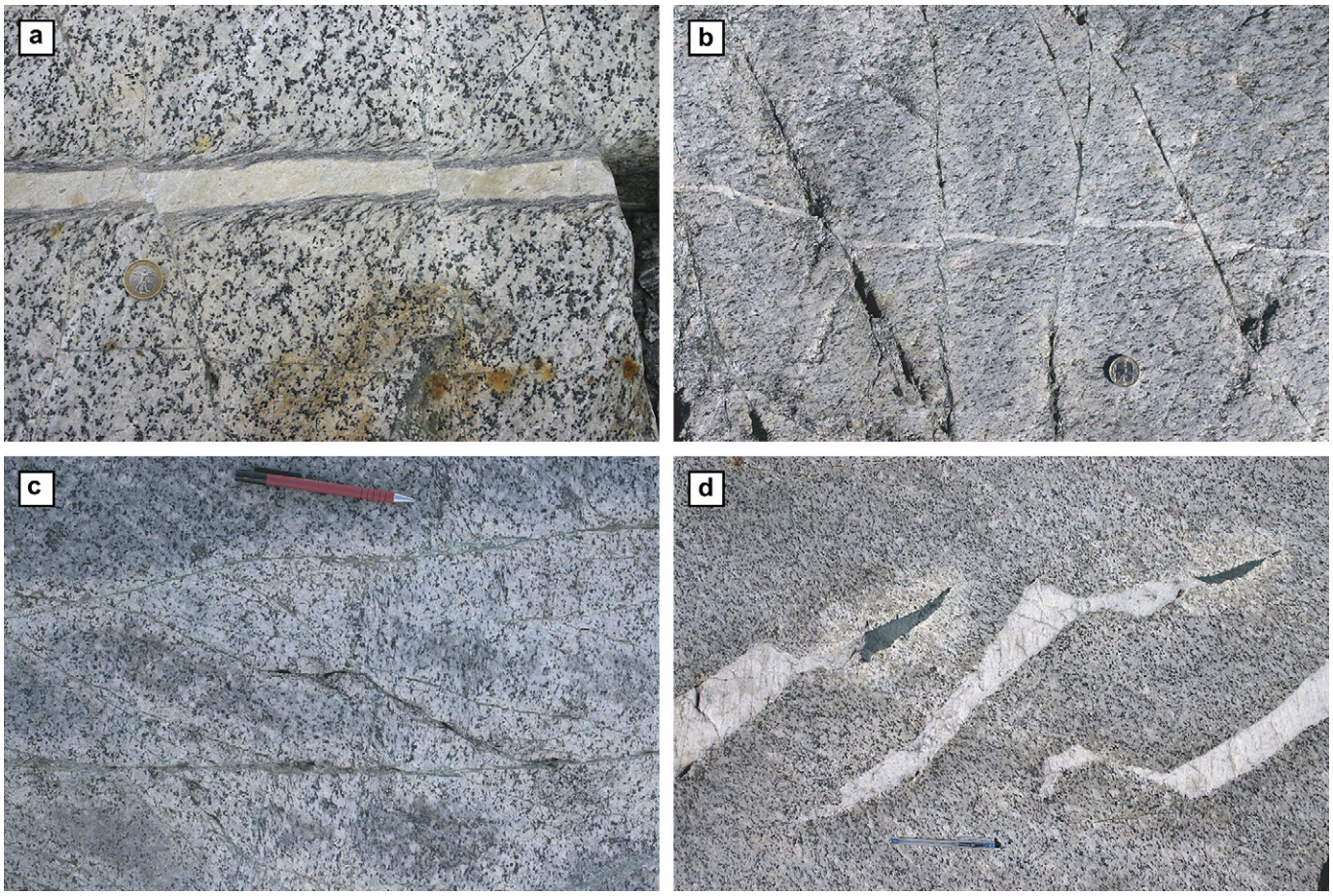

Fig. 17. Late epidote–chlorite (±quartz, ±zeolite) fractures. (a) Overprint of epidote–chlorite conjugate shear fractures on an aplite, with an amphibolite facies paired shear zone developed on its boundaries. Looking down, top to W; GPS coordinates: N 46°58′33.1″, E 11°47′52.7″; coin (2.3 cm in diameter) for scale. (b) Conjugate sets of epidote–chlorite shear fractures displacing an aplite dyke. Note the relatively small intersection angle between the two sets. Looking down, top to N; GPS coordinates: N 46°58′27.6″, E 11°47′45.3″; coin (2.3 cm in diameter) for scale. (c) Bleaching of the granodiorite surrounding epidote–chlorite fractures. Looking down, top to W; GPS coordinates: N46°58′23.13″, E 11°47′47.75″; pen (14 cm long) for scale. (d) Chlorite-filled veins extending from the tips of former higher temperature quartz veins in an en-echelon array. Note that the bleaching of the granodiorite is only developed around the chlorite veins. Looking down, top to E; GPS coordinates: N 46°58′28.2″, E 11°47′47.6″; pen (13 cm long) for scale.

indicates a principal compressive stress direction σ_1 trending ca. 350°, with the intermediate stress axis σ_2 near vertical. This is identical to the principal stress orientations obtained by Mancktelow et al. (2001 figure 5) from faults related to the Periadriatic Fault system in the Mauls–Plattspitz–Ochsensprung area, some 20–30 km SW of the Neves area. It is also approximately the same as that obtained in Section 7 above for the earlier development of ductile shear zones and high-grade veins under amphibolite facies metamorphic conditions. The regional kinematics have therefore remained the same during exhumation and cooling.

9. Discussion

9.1. Age of fracturing and veining

In the Neves area, shear zones exploited fractures that have been commonly infiltrated by fluids to develop veins and adjacent bleaching haloes. However, as noted above, the relative (and absolute) age of formation of the different fractures and of the associated fluid infiltration with respect to ductile shearing is uncertain. From direct field observations, it is clearly established that the formation of quartz (±biotite, ±calcite, ± plagioclase) veins is coeval with the ductile deformation. In fact, opening features of veins (e.g. pull aparts and wings) in the weakly deformed domains are consistent with the bulk kinematic framework and indicate the same sense of shear as their ductile overprint. There is direct evidence that some veins filled new fractures developed during the ductile deformation. For example, undeformed veins cut across mylonites (Fig. 11f), and veins within ''undeformed'' granodiorite cut straight through sheared fractures (Fig. 11d). Small quartz-calcite veins develop cyclically in an orientation subparallel to the inferred principal compressive stress axis σ_1 and are then rotated synkinematically. This sequential nucleation of veins is well recorded in Fig. 11g. Direct overprinting of rotated and ductilely deformed veins by new veins demonstrates that (1) veins fill newly produced fractures and (2) vein/fracture opening occurred continuously during progressive strain.

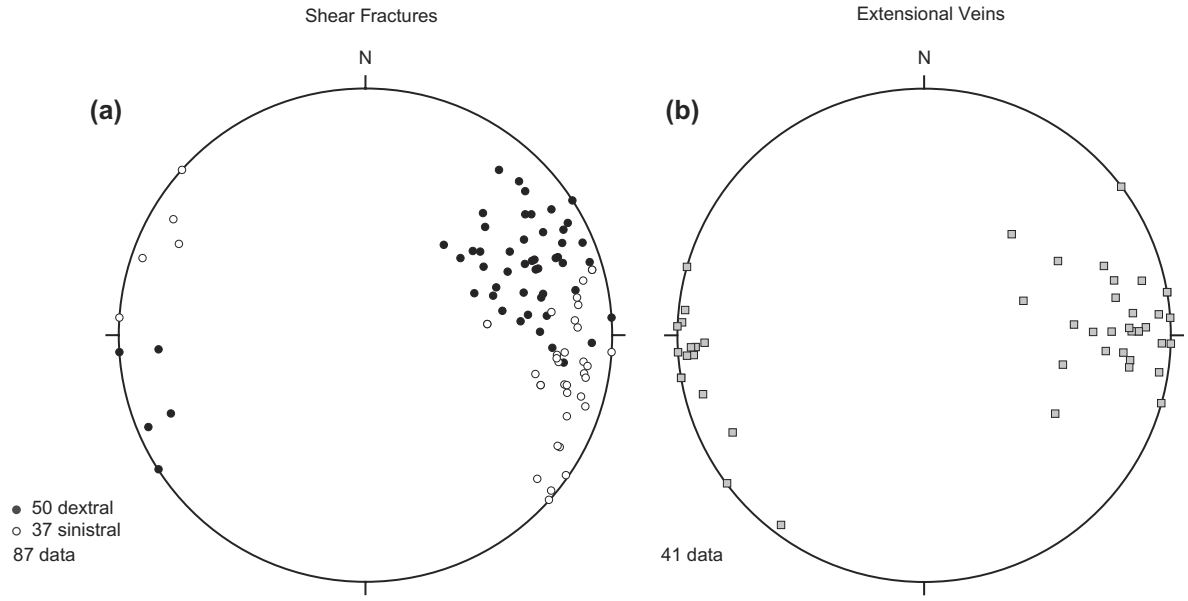

Fig. 18. Orientation data for late fractures and veins, plotted in stereographic projection (lower hemisphere). Typical new minerals associated with these structures are chlorite, epidote, quartz and zeolite. A distinction is made between discrete faults and cataclastic zones with a clear sinistral or dextral offset (a), and fractures and veins without apparent offset (b). Note that the switch between dextral and sinistral faults and the mean orientation for the extensional veins of 355°/79° W (strike/dip) both indicate that σ_1 during this late fracturing was very close in orientation to that inferred for the earlier amphibolite facies deformation.

The Alpine age of the quartz-rich veins was already recognized by Cesare et al. (2001), who made a detailed petrographical and fluid inclusion study of the quartz-biotite-plagioclase veins in the Neves area. From their fluid-inclusion results, they concluded that the fluid composition was quite homogeneous from one vein to the next, with rather high salinities (3–7 mol%) and with the volatile phase dominantly CO_2 (3–12 mol%). They estimated the trapping conditions as 550–600 °C and 3.5–7.5 kbar, corresponding to peak conditions of Alpine metamorphism in the Tauern window, which was dated at ca. 30 Ma by Christensen et al. (1994). This time corresponds to the intrusion of dykes and plutons of the so-called Periadriatic intrusives (e.g. Salomon, 1897; von Blanckenburg et al., 1998), which are spatially distributed along the Periadriatic fault, a regional dextral transpressive structure that also initiated around this time (Schmid et al., 1989; Berger et al., 1996; Müller et al., 2000, 2001; Mancktelow et al., 2001; Rosenberg, 2004).

Quartz–calcite–biotite–plagioclase veins crosscut epidote and biotite-bearing fractures or the derived single and paired shear zones, whereas the opposite has never been observed. It is also significant that, in most cases, the quartz veins are not overprinted by fractures and shear zones but terminate against these structures, indicating that the fractures and shear zones were pre-existing structures. Fractures, more-or-less filled with epidote or biotite, form the precursor nucleation site for subsequent localization of ductile shear zones. These observations suggest that fracturing and associated vein filling (predominantly by epidote and biotite) predate the development of quartz veins and, possibly, the overall onset of ductile deformation. The difference in mineral filling between the epidote-rich veins and quartz-calcite-biotite-plagioclase veins points to a difference in P-T-fluid conditions during vein formation that can either be due to distinct episodes of fluid infiltration or to differences in fluid composition associated with locally varying fluid/rock ratios in a single episode (Rolland et al., 2003). The orientation of the two vein sets is in general also different, with most epidote veins striking E–W and most quartz veins N–S, although this spatial distinction is not without exceptions. In most paired shear zones, the sense of shear on the central fracture/vein is the same as that of the flanking shear zones (cf. Mancktelow and Pennacchioni, 2005, figure 7). However, in a significant minority of cases with ca. E–W strike, the opposite is observed: the central fracture has a sinistral offset, whereas the flanking shear zones are dextral (Fig. 5c). Epidote-rich alteration occurs in pull-apart zones related to sinistral shear (Fig. 5d) and is clearly coeval with this shearing. Regionally, in the Eastern Alps south of the Tauern Window, there is an inversion in the sense of the ca. E–W-striking transcurrent component from dominantly sinistral (the so-called DAV mylonites) to dominantly dextral (the Periadriatic Fault system) at around 30 Ma (Mancktelow et al., 2001). As noted above, this time has been interpreted by previous authors to correspond to the peak of the Tauern metamorphism (Christensen et al., 1994) and to the development of quartz-calcite-biotite-plagioclase veins (Cesare et al., 2001). A correlation with the regional kinematics is speculative, but it would imply that at least some of the E–W fractures were already present and reactivated under the pre-30 Ma kinematic regime dominated by sinistral strike-slip. In summary, the very distinct mineralogical difference between the two vein sets, the difference in orientation, and the field observation that epidote-rich veins are crosscut by quartz-rich veins but not vice-versa are strong indications that the two vein systems were not coeval but developed sequentially. The time between is indeterminate and it is even possible that the epidote-filled ca.

E–W-striking fractures could be inherited joints developed during cooling of the pre-Alpine intrusion.

9.2. Bulk kinematics of the Neves area

The heterogeneous, localized deformation in the Neves area is dominated by shear zones on all scales, from sub-millimetre to tens of metres or (on the southern boundary) kilometres in width. However, on the scale of the whole area, the orientation and kinematics of the individual structures indicate that the bulk deformation within this generally low strain domain was effectively coaxial, as established above in Section 7. Clearly this is not the case within individual shear zones, but the measurements presented in Figs. 15 and 16 were either taken in low strain domains between shear zones or represent the orientation of the shear zones themselves. Measurements were rarely taken within shear zones, either because features did not transect such zones (e.g. most quartz veins) or were so strongly overprinted in the shear zones that they were no longer recognizable. Some quartz veins also transect E–W dextral shear zones without significant deformation but the orientation of these veins obviously does not reflect the finite strain within the shear zones themselves. Likewise, the orientation of the bulk foliation corresponds to that in the volumetrically predominant areas between shear zones. As a consequence of the strong localization, foliation within shear zones generally makes only a (very) small angle with the zone boundary and it was this boundary orientation that was recorded, using the slight obliquity, where discernible, to establish the sense of shear.

An effectively coaxial deformation within the low strain domains is also indicated by the observed geometry and kinematics of individual structures. The dominant shear zones in the study area, both in number and in the width attained, are dextral and strike ca. E–W. The lamprophyre$_2$ dykes also strike ca. E–W and show a strong dextral shear overprint. The shear component in the intervening regions might therefore also be expected to be dextral. As noted above, precursor structures localizing shear cover effectively the complete range of orientations (Fig. 16). In a bulk non-coaxial regime with a dextral shear component, planes with an original orientation close to the instantaneous shortening direction (ISA_1, e.g. Passchier and Trouw, 2005) and an initial dextral shear component are expected to rotate clockwise and enter the field of sinistral shear with increasing deformation. This would result in (1) overprinting of sinistral on dextral shear for structures in an orientation slightly rotated clockwise from the shortening direction, which is not observed with very few exceptions, (2) a less clear-cut separation between dextral and sinistral structures (in the cumulative plot of Fig. 16, the transition from dextral to sinistral shear zones is remarkably sharp), and (3) an asymmetric distribution of poles to foliation with respect to the inferred ISA_1 direction, which in contrast is rather symmetric (Fig. 16). Precursors oriented at a high angle to the ISA_1 direction but with an initial sinistral sense should also rotate clockwise and, on passing the perpendicular position, show a subsequent overprint of sinistral by dextral shear. However, as shown by the reactivated fractures indicated by black arrows on Fig. 4, this is not observed. Rather, there is a consistent inversion in the shear sense reflecting the slight change in orientation of the fractures in a clockwise sense "across" the strike direction perpendicular to the inferred ISA_1 (ca. 345°).

As discussed by Ramsay and Graham (1970) and Cobbold (1977a), strain compatibility requires that elongate banded structures, such as shear zones, can only be due to a component of heterogeneous simple shear and/or volume change superimposed on a background homogeneous strain. As discussed above, in the Neves area, the background homogeneous strain in the low-strain areas between shear zones is effectively coaxial. This strain is also present in the shear zones, which implies that the dominant E–W shear zones must be transpressional or "stretching faults" (Means, 1989) whose length increases with time, even without any active propagation of the shear zone tips. Extension parallel to E–W shear zones produces lobate–cuspate instabilities in the boundary between (dextrally) sheared E–W lamprophyre$_2$ and the adjacent granodiorite, with the regularly spaced lamprophyre cusps commonly localizing tapered quartz veins that extend into the granodiorite (Fig. 13). As summarized in the cartoon of Fig. 19,

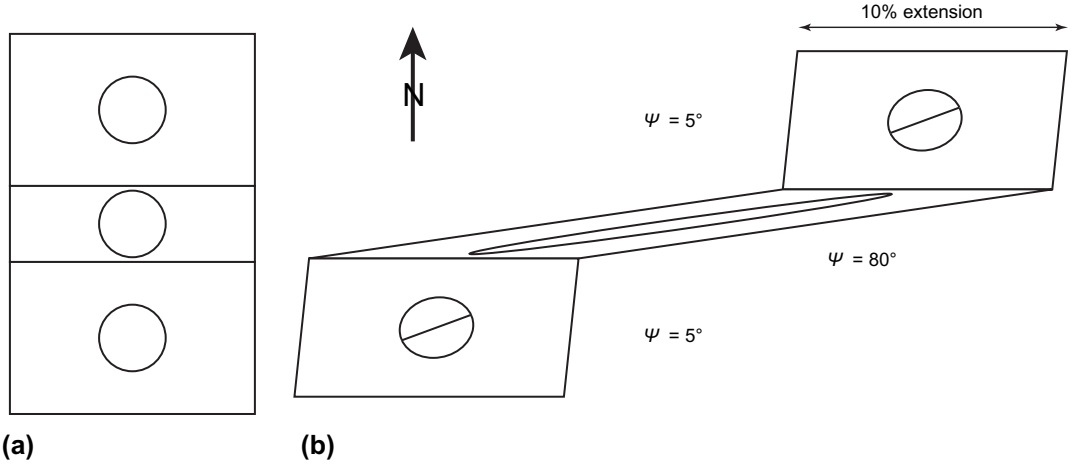

Fig. 19. Cartoon of strain partitioning between shear zones and low-strain domains, with the shear angle ψ and bulk background pure shear extension indicated. The values are only illustrative, but the chosen combination of 10% homogeneous extension and $\psi = 5°$ in the low strain domains would produce a (weak) bulk foliation of the same general orientation as that observed in the Neves area.

the overall deformation is interpreted to be one of dextral transpression. In this model, the shear component is localized in ca. E–W-striking shear zones on varying scales, whereas the intervening low-strain domains reflect the effectively coaxial background homogeneous component. This coaxial bulk strain component is accommodated both by diffuse deformation, reflected in the bulk solid-state foliation with strike ca. 075°, and by a distributed network of localized shear zones with foliation at a low angle to the shear zone boundaries (Fig. 19b). Bulk extension of the weaker, dextrally sheared E–W lamprophyre$_2$ will be accompanied by stress refraction, with the principal stress axes making a larger angle to rheological boundary in the stronger granodiorite and a lower angle in the dyke (Strömgård, 1973; Treagus, 1973; Mancktelow, 1993). The average regional σ_1 direction during dextral transpression may therefore be more toward the NW than the direction 345° determined by our analysis in the Neves low-strain domain.

9.3. Quartz vein orientation, geometry and kinematics

The initial fracture associated with vein formation is usually assumed to be an extensional or mode I crack (e.g. Ramsay and Huber, 1983, figure 3.21; Olson and Pollard, 1991), as also implied by the initial orientation of first-formed fibres in fibrous veins (Durney and Ramsay, 1973). However, in the Neves area, the large majority of quartz veins within low strain domains have geometric features and ductile fabrics indicating that vein opening, filling and deformation involved transtensive sinistral shearing parallel to the vein. A sinistral ductile overprint is expected, in a bulk dextral shear regime, for veins that opened as extensional fractures, with a strike direction parallel to the principal compressive stress σ_1 (i.e. ca. 345° in the current case), and were subsequently rotated clockwise into the quadrant where the vein-parallel resolved shear stress is sinistral. The sinistral opening features of veins could thereby be interpreted in terms of (1) initiation as mode I fractures in the direction of the bulk σ_1, and (2) continued opening within the domain of sinistral reactivation during rotation related to a bulk dextral shear strain. Alternatively, the winged quartz veins could develop during simple shear deformation by exploiting synkinematic synthetic (R) and antithetic (R′) Riedel fractures, as recently suggested by Coelho et al. (2006), based on observation of natural vein occurrences in Namibia and analogue modelling. This interpretation is rather attractive, especially considering the similarity between the vein pattern outlined in the map of Fig. 9 and the experimentally produced vein arrays in Coelho et al. (2006). However, the vein appendages in the current area are more directly comparable to the wing geometries described by Willemse and Pollard (1998), commonly showing an arcuate horn-shaped geometry with the vein tips pointing toward the interpreted direction of σ_1 (345°). In contrast, the pennant veins described by Coelho et al. (2006) typically have straight boundaries determined by the R–R′ planes. In either case, such models to explain the dominance of sinistral veins assume a bulk component of dextral non-coaxial deformation in the low-strain domains. However, as discussed above, the overall kinematic dataset suggests instead that the bulk deformation within the low strain domains was effectively coaxial.

The plots of Fig. 15c,d show that quartz veins have a significant range in orientation but with a maximum around a ca. N–S strike. In the field, quartz veins showing no evidence for shear are approximately orthogonal to the bulk foliation and have a maximum in orientation of 344°/074°E (strike/dip). This orientation is parallel to the inferred σ_1 (Fig. 16) and such quartz veins can be readily explained as filled mode I fractures. Other quartz veins, typically showing a sinistral shear sense, have a clear spatial association with E–W-striking shear zone boundaries and an orientation striking ca. N–S to NNE–SSW, which is close to perpendicular to the adjacent shear zones (Figs. 9, 12, 14). As noted above, some of these veins can be directly linked to lobate–cuspate structures developed due to mechanical instability of the extending rheological interface between strong granodiorite and weak lamprophyre$_2$ (Fig. 13). This is similar to the type I boudin parting surfaces described by Hanmer (1986) and to the foliation boudinage mechanism for development of winged quartz veins invoked by Swanson (1992). Overall, the alternation of weak fractures, shear zones and lamprophyre$_2$ with stronger low-strain domains of granodiorite could produce a significant bulk anisotropy. This would lead to local (and perhaps transient) stress rotation (e.g. Kocher and Mancktelow, 2006), controlling the location and orientation of the synkinematic fractures filled with quartz. The observed range in quartz vein orientations could reflect a combination of (1) different initial opening directions reflecting different local degrees of anisotropy and control by mechanical instability developed at stretched rheological boundaries, (2) different amounts of passive rotation of veins formed in different orientations and at different times, and (3) different degrees of precursor control. For example, some quartz veins showing dextral shear (6 out of 22) are clearly intruded along pre-existing aplite dykes and their orientation is simply related to that of the precursor compositional heterogeneity. The uncertainty in establishing the dominant mechanism(s) controlling synkinematic fracturing and vein formation is in part related to the difficulty in estimating the amount of bulk strain in the low strain domains. However, the field observations clearly establish that the synkinematic fractures initiated with variable orientations, reflecting the compositional heterogeneity, and that not all the measured variability in orientation can be attributed to variable amounts of subsequent rotation.

9.4. Precursor control of shear zones and fractures

Shear zones in the Neves area always initiate on, and strictly follow, approximately planar precursors such as fractures, layers or boundaries and have never been observed to propagate away from or beyond the tip of such precursors. The strain associated with the displacement gradient at the end of such shear zones of fixed length is accommodated by broader zones of distributed deformation and foliation development and by local fracturing. It should be noted, however, that no ends of major shear zones with tens of metres

displacement are located within the current study area and no information is therefore available on how accommodation is achieved when displacements are large. If the smaller contractional bridges commonly observed are models of the larger scale, then transfer of displacement occurs by linkage via broader ductile contractional bridge zones (Pennacchioni, 2005, figure 7). With increasing shear, the tips of shear zones move away from each other, the bridge zones become more elongated, thinned and strongly foliated, and the angle between the tips of the stepped shear zones decreases, so that an effectively continuous single shear zone of high strain is developed (Pennacchioni, 2005). Increasing strain is reflected in a broadening of the shear zones to include more of the adjacent host. In fact, shear zones are most localized during initiation along the precursor fracture or compositional boundary and actually broaden rather than localize with increasing bulk strain. This implies that shearing both along the discrete fractures and within the flanking shear zones involves strain hardening rather than weakening. Shearing localizes on the boundary of stronger layers, such as aplite dykes or bleached haloes developed to either side of fractures, but occurs in a relatively homogeneous manner within weak layers, such as the lamprophyres and quartz veins. It should also be emphasized that all precursor structures with a shear stress component acting on them are reactivated in shear, although the amount of shear is variable. This is consistent with a viscous rheology during shearing, without a specific yield strength. The shear strain rate is proportional to the shear stress parallel to the controlling precursor surface and is only zero if the resolved shear stress on the surface is also zero.

In marked contrast to the shear zones, fractures are not invariably controlled by precursor structures and there are many examples of fractures crossing aplite dykes and lamprophyres at a small angle, without regard for the boundary (e.g. Fig. 3d). Extensional quartz veins and the tips of wing cracks also develop in an orientation consistent with the interpreted σ_1 direction, without regard for earlier fractures or compositional boundaries. However, as discussed above, there is also a tendency for quartz veins to develop approximately perpendicular to rheological and lithological boundaries, such as shear zones and lamprophyres. In some cases, there is also a clear spatial relation to steps in the intrusive dyke boundary and to regular lobate–cuspate structures on the boundary of extended and sheared dykes.

10. Conclusions

Granitoid plutons have typically been considered as relatively homogeneous and isotropic bodies, with the lack of a pervasive layering precluding the development of buckle folds and thus promoting the development of heterogeneous ductile shear zones. However, intrusive bodies are in fact characterized by ubiquitous heterogeneities due to intrusive contacts and joints developed during cooling or brittle deformation. Subsequent ductile deformation under elevated metamorphic conditions is controlled by these pre-existing features. Localization concentrates at the boundaries of strong layers (e.g. aplite and pegmatite dykes, bleached haloes along joints) and within weak layers (e.g. lamprophyre dykes, quartz veins, biotite-rich healed joints). Discontinuities are sheared whatever their orientation, with the sense and amount of displacement determined by the resolved shear stress. The observation that shear reactivation occurs even when the component of resolved shear stress for the particular orientation is very small is consistent with an effectively viscous rheology during ductile shearing, without a specific yield stress.

Our observations show that shear zones do not develop spontaneously in macroscopically homogeneous rock and do not propagate beyond the termination of isolated precursors or deviate away from compositional or structural boundaries. This is in stark contrast to brittle fractures, which may ignore pre-existing structures, locally crosscutting boundaries at low angles. Development of ductile shear zones in homogeneous intact rock is therefore always dependent on precursor development of a brittle fracture. It follows that accommodation of strain incompatibilities during bulk deformation of a shear zone network is accomplished by more diffuse deformation and by synkinematic brittle fracture and veining, which may subsequently be exploited by localized ductile shear. During the same ongoing deformation history, pre-existing ductile shear zones can thereby be crosscut by later brittle fractures and veins.

Compatibility problems are particularly evident at the intersection of conjugate shear zones. In contrast to brittle conjugate faults in rigid blocks, ductile shear zones can be active synchronously, with the development of a typical thinned intersection zone marked by a strongly developed foliation perpendicular to the shortening direction and parallel to the regional bulk foliation.

A shear zone network cannot efficiently accommodate large bulk strains and deformation must spread into the intervening blocks. As established in this study, localizing deformation in granitoids requires a structural discontinuity as precursor, and our observations are that subsequent fracturing is limited in extent. Large bulk deformation therefore can only be achieved by more diffuse strain involving broadening of initially highly localized shear zones. Strain therefore spreads rather than localizes with progressive deformation.

Acknowledgements

We particularly thank Roland and Anna Gruber, the guardians of the Alpine hut Chemnitzer Hütte, for their warm and friendly hospitality during the field work. The research was funded by the University of Padova: Ricerca Scientifica fondi quota ex 60% (60A05-3129/05 and 60A05-3770/06) and by internal research funds of the ETH Zürich. Reviews by Mark Swanson and an anonymous reviewer are gratefully acknowledged.

Supplementary data

Supplementary information associated with this article can be found in the online version, at doi:10.1016/j.jsg.2007.06.002.

References

Aydin, A., Nur, A., 1982. Evolution of pull-apart basins and their scale independence. Tectonics 1, 91–105.

Behrmann, J.H., 1988. Crustal-scale extension in a convergent orogen: the Sterzing-Steinach mylonite zone in the Eastern Alps. Geodinamica Acta 2, 63–73.

Berger, A., Rosenberg, C., Schmid, S.M., 1996. Ascent, emplacement and exhumation of the Bergell pluton within the Southern Steep Belt of the Central Alps. Schweizerische Mineralogische und Petrographische Mitteilungen 76, 357–382.

Berthé, D., Choukroune, P., Jegouzo, P., 1979. Orthogneiss, mylonite and non coaxial deformation of granites: the example of the South Armorican Shear Zone. Journal of Structural Geology 1, 31–42.

Bowden, P.B., 1970. A criterion for inhomogeneous plastic deformation. Philosophical Magazine 22, 455–462.

Brun, J.P., Cobbold, P.R., 1980. Strain heating and thermal softening in continental shear zones: a review. Journal of Structural Geology 2, 149–158.

Burg, J.P., Laurent, Ph., 1978. Strain analysis of a shear zone in a granodiorite. Tectonophysics 47, 15–42.

Bürgmann, R., Pollard, D.D., 1992. Influence of the state of stress on the brittle-ductile transition in granitic rock: evidence from fault steps in the Sierra Nevada, California. Geology 20, 645–648.

Bürgmann, R., Pollard, D.D., 1994. Strain accommodation about strike-slip fault discontinuities in granitic rocks under brittle-to-ductile conditions. Journal of Structural Geology 16, 1655–1674.

Carreras, J., Cobbold, P.R., Ramsay, J.G., White, S.H., 1980. Shear Zones in Rocks. Journal of Structural Geology 2, 1–287.

Casey, M., 1980. Mechanics of shear zones in isotropic dilatant materials. Journal of Structural Geology 2, 143–147.

Cesare, B., Poletti, E., Boiron, M.-C., Cathelineau, M., 2001. Alpine metamorphism and veining in the Zentralgneis Complex of the SW Tauern Window: a model of fluid-rock interactions based on fluid inclusions. Tectonophysics 336, 121–136.

Cesare, B., Rubatto, D., Hermann, J., Barzi, L., 2002. Evidence for Late Carboniferous subduction-type magmatism in mafic-ultramafic cumulates of the SW Tauern window (Eastern Alps). Contributions to Mineralogy and Petrology 142, 449–464.

Christensen, J.N., Selverstone, J., Rosenfeld, J.L., DePaolo, D.J., 1994. Correlation of Rb-Sr geochronology of garnet growth histories from different structural levels within the Tauern Window, Eastern Alps. Contributions to Mineralogy and Petrology 118, 1–12.

Christiansen, P.P., Pollard, D.D., 1997. Nucleation, growth and structural development of mylonitic shear zones in granitic rocks. Journal of Structural Geology 19, 1159–1172.

Cloos, E., 1955. Experimental analysis of fracture patterns. Geological Society of America Bulletin 66, 241–256.

Cobbold, P.R., 1977a. Description and origin of banded deformation structures. I. Regional strain, local perturbations, and deformation bands. Canadian Journal of Earth Sciences 14, 1721–1731.

Cobbold, P.R., 1977b. Description and origin of banded deformation structures. II. Rheology and the growth of banded perturbations. Canadian Journal of Earth Sciences 14, 2510–2523.

Coelho, S., Passchier, C., Marques, F., 2006. Riedel-shear control on the development of pendant veins: field example and analogue modelling. Journal of Structural Geology 28, 1658–1669.

De Vecchi, G.P., Mezzacasa, G., 1986. The Pennine basement and cover units in the Mesule group (southwestern Tauern window). Memorie di Scienze Geologiche 38, 365–392.

D'Amico, C., 1974. Hercynian plutonism in the Alps. A report 1973-74 (Relazione ufficiale). Memorie della Società Geologica Italiana 13, 49–118.

Durney, D.W., Ramsay, J.G., 1973. Incremental strains measured by syntectonic crystal growth. In: DeJong, K.A., Scholten, R. (Eds.), Gravity and Tectonics. Wiley, New York, pp. 67–96.

Finger, F., Frasl, G., Haunschmid, B., Lettner, H., von Quadt, A., Schermaier, A., Schindlmayr, A.O., Steyrer, H.P., 1993. The Zentralgneise of the Tauern Window (Eastern Alps): insight into an intra-Alpine Variscan Batholith. In: von Raumer, J.F., Neubauer, F. (Eds.), Pre-Mesozoic Geology of the Alps. Springer, Berlin, pp. 375–391.

Flügel, H.W., Faupl, P., 1987. Geodynamics of the Eastern Alps. Deuticke, Vienna.

Freund, R., 1974. Kinematics of transform and transcurrent faults. Tectonophysics 21, 93–134.

Freund, R., Merzer, A.M., 1976. Formation of rift valleys and their zigzag fault patterns. Geological Magazine 113, 561–568.

Friedrichsen, H., Morteani, G., 1979. Oxygen and hydrogen isotope studies on minerals from alpine fissures and their gneissic host rocks. Western Tauern Window (Austria). Contributions to Mineralogy and Petrology 70, 149–152.

Frisch, W., Vavra, G., Winkler, M., 1993. Evolution of Penninic basement of the Eastern Alps. In: von Raumer, J.F., Neubauer, F. (Eds.), Pre-Mesozoic Geology of the Alps. Springer, Berlin, pp. 349–360.

Fügenschuh, B., Seward, D., Mancktelow, N., 1997. Exhumation in a convergent orogen: the western Tauern Window. Terra Nova 9, 213–217.

Fusseis, F., Handy, M.R., Schrank, C., 2006. Networking of shear zones at the brittle-to-viscous transition (Cap de Creus, NE Spain). Journal of Structural Geology 28, 1228–1243.

Gamond, J.F., 1983. Displacement features associated with fault zones: a comparison between observed examples and experimental models. Journal of Structural Geology 5, 33–45.

Gamond, J.F., 1987. Bridge structures as sense of displacement criteria in brittle fault zones. Journal of Structural Geology 9, 609–620.

Genter, M.A., 1993. Analytical and numerical considerations on the initiation and propagation of ductile shear zones in elastic-thermo-viscous power law materials. PhD Thesis, ETH Zürich, Switzerland.

Grujic, D., Mancktelow, N.S., 1998. Melt-bearing shear zones: analogue experiments and comparison with examples from southern Madagascar. Journal of Structural Geology 20, 673–680.

Guermani, A., Pennacchioni, G., 1998. Brittle precursors of plastic deformation in a granite: an example from the Mont Blanc massif (Helvetic, western Alps). Journal of Structural Geology 20, 135–148.

Hanmer, S., 1986. Asymmetrical pull-aparts and foliation fish as kinematic indicators. Journal of Structural Geology 8, 111–122.

Hoernes, S., Friedrichsen, H., 1974. Oxygen isotope studies on metamorphic rocks of the western Hohe Tauern area (Austria). Schweizerische Mineralogische und Petrographische Mitteilungen 54, 769–788.

Ildefonse, B., Mancktelow, N.S., 1993. Deformation around rigid particles: the influence of slip at the particle/matrix interface. Tectonophysics 221, 345–359.

Ingles, J., Lamouroux, C., Soula, J.-C., Guerrero, N., Debat, P., 1999. Nucleation of ductile shear zones in a granodiorite under greenschist facies conditions, Néouvielle massif, Pyrenees, France. Journal of Structural Geology 21, 555–576.

Kaus, B.J.P., Podladchikov, Y.Y., 2006. Initiation of localized shear zones in viscoelastoplastic rocks. Journal of Geophysical Research 111, BO4412, doi:10.1029/2005JB003652.

Kocher, T., Mancktelow, N.S., 2006. Flanking structure development in anisotropic viscous rock. Journal of Structural Geology 28, 1139–1145.

Mancktelow, N.S., 1993. Tectonic overpressure in competent mafic layers and the development of isolated eclogites. Journal of Metamorphic Geology 11, 801–812.

Mancktelow, N.S., 2002. Finite-element modelling of shear zone development in viscoelastic materials and its implications for localisation of partial melting. Journal of Structural Geology 24, 1045–1053.

Mancktelow, N.S., 2006. How ductile are ductile shear zones? Geology 34, 345–348.

Mancktelow, N.S., Pennacchioni, G., 2005. The control of precursor brittle fracture and fluid-rock interaction on the development of single and paired ductile shear zones. Journal of Structural Geology 27, 645–661.

Mancktelow, N.S., Stöckli, D.F., Grollimund, B., Müller, W., Fügenschuh, B., Viola, G., Seward, D., Villa, I.M., 2001. The DAV and Periadriatic fault systems in the Eastern Alps south of the Tauern window. International Journal of Earth Sciences 90, 593–622.

Mandal, N., Misra, S., Samanta, S.K., 2004. Role of weak flaws in nucleation of shear zones: an experimental and theoretical study. Journal of Structural Geology 26, 1391–1400.

Means, W.D., 1989. Stretching faults. Geology 17, 893–896.

Morgenstern, N.R., Tchalenko, J.S., 1967. Microscopic structures in kaolin subjected to direct shear. Géotechnique 17, 309–328.

Morteani, G., 1974. Petrology of the Tauern Window, Austrian Alps. Fortschritte der Mineralogie 52, 195–220.

Müller, W., Mancktelow, N.S., Meier, M., 2000. Rb-Sr microchrons of synkinematic mica in mylonites: an example from the DAV fault of the Eastern Alps. Earth and Planetary Science Letters 180, 385–397.

Müller, W., Prosser, G., Mancktelow, N.S., Villa, I.M., Kelley, S.P., Viola, G., Oberli, F., 2001. Geochronological constraints on the evolution of the Periadriatic Fault System (Alps). International Journal of Earth Sciences 90, 623–653.

Olson, J.E., Pollard, D.D., 1991. The initiation and growth of en echelon veins. Journal of Structural Geology 13, 595–608.

Passchier, C.W., Trouw, R.A.J., 2005. Microtectonics, second ed. Springer, Berlin.

Pennacchioni, G., 2005. Control of the geometry of precursor brittle structures on the type of ductile shear zone in the Adamello tonalites, Southern Alps (Italy). Journal of Structural Geology 27, 627–644.

Poirier, J.P., 1980. Shear localization and shear instability in materials in the ductile field. Journal of Structural Geology 2, 135–142.

Ramsay, J.G., Allison, I., 1979. Structural analysis of shear zones in an alpinised Hercynian granite (Maggia Lappen, Pennine Zone, Central Alps). Schweizerische Mineralogische und Petrographische Mitteilungen 59, 251–279.

Ramsay, J.G., Graham, R.H., 1970. Strain variation in shear belts. Canadian Journal of Earth Sciences 7, 786–813.

Ramsay, J.G., Huber, M.I., 1983. The Techniques of Modern Structural Geology. Strain Analysis, Volume 1. Academic Press, London.

Ramsay, J.G., Huber, M.I., 1987. The Techniques of Modern Structural Geology. Folds and Fractures, Volume 2. Academic Press, London.

Richard, P.D., Naylor, M.A., Koopman, A., 1995. Experimental models of strike-slip tectonics. Petroleum Geoscience 1, 71–80.

Riedel, W., 1929. Zur Mechanik geologischer Brucherscheinungen. Zentralblatt für Mineralogie, Geologie und Paläontologie. B, 354–368.

Rolland, Y., Cox, S., Boullier, A.-M., Pennacchioni, G., Mancktelow, N., 2003. Rare earth and trace element mobility in mid-crustal shear zones: insights from the Mont Blanc Massif (Western Alps). Earth and Planetary Science Letters 214, 203–219.

Rosenberg, C.L., 2004. Shear zones and magma ascent: a model based on a review of the Tertiary magmatism in the Alps. Tectonics 23, TC3002, doi:10.1029/2003TC001526.

Salomon, W., 1897. Über Alter, Lagerungsform und Entstehungsart der periadriatischen granitischkörnigen Massen. Hölder, Vienna.

Schmid, S.M., Aebli, H.R., Heller, F., Zingg, A., 1989. The role of the Periadriatic Line in the tectonic evolution of the Alps. In: Coward, M.P., Dietrich, D., Park, R.G. (Eds.), Alpine Tectonics. Special Publication 45. Geological Society, London, pp. 153–171.

Segall, P., Pollard, D.D., 1980. Mechanics of discontinuous faults. Journal of Geophysical Research 85, 4337–4350.

Segall, P., Pollard, D.D., 1983. Nucleation and growth of strike slip faults in granite. Journal of Geophysical Research 88, 555–568.

Segall, P., Simpson, C., 1986. Nucleation of ductile shear zones on dilatant fractures. Geology 14, 56–59.

Selverstone, J., 1985. Petrologic constraints on imbrication, metamorphism, and uplift in the SW Tauern Window, Eastern Alps. Tectonics 4, 687–704.

Selverstone, J., 1988. Evidence for east-west crustal extension in the Eastern Alps: implications for the unroofing history of the Tauern Window. Tectonics 7, 87–105.

Selverstone, J., Spear, F.S., Franz, G., Morteani, G., 1984. High-pressure metamorphism in the SW Tauern Window, Austria: P-T paths from hornblende-kyanite-staurolite schists. Journal of Petrology 25, 501–531.

Strömgård, K.-E., 1973. Stress distribution during formation of boudinage and pressure shadows. Tectonophysics 16, 215–248.

Swanson, M.T., 1992. Late Acadian-Alleghenian transpressional deformation: evidence from asymmetric boudinage in the Casco Bay area, coastal Maine. Journal of Structural Geology 14, 323–341.

Takagi, H., Goto, K., Shigematsu, N., 2000. Ultramylonite bands derived from cataclasite and pseudotachylyte in granites, northeast Japan. Journal of Structural Geology 22, 1325–1340.

Tchalenko, J.S., 1970. Similarities between shear zones of different magnitudes. Geological Society of America Bulletin 81, 1625–1640.

Tchalenko, J.S., Ambraseys, N.N., 1970. Structural analysis of the Dasht-e Bayaz (Iran) earthquake fractures. Geological Society of America Bulletin 81, 41–60.

Treagus, S.H., 1973. Buckling stability of a viscous single-layer system, oblique to the principal compression. Tectonophysics 19, 271–289.

Tullis, J., Dell' Angelo, L., Yund, R.A., 1990. Ductile shear zones from brittle precursors in feldspathic rocks: the role of dynamic recrystallization. In: Duba, A., Durham, W., Handin, J., Wang, H. (Eds.), The Brittle-Ductile Transition: The Heard volume. American Geophysical Union Monograph, vol. 56, pp. 67–82.

Viola, G., Mancktelow, N.S., Seward, D., 2001. Late Oligocene-Neogene evolution of Europe-Adria collision: new structural and geochronological evidence from the Giudicarie fault system (Italian Eastern Alps). Tectonics 20, 999–1020.

Vissers, R.L.M., Drury, M.R., Strating, E.H.H., Vanderwal, D., 1991. Shear zones in the upper mantle—a case-study in an Alpine lherzolite massif. Geology 19, 990–993.

von Blanckenburg, F., Villa, I.M., Baur, H., Morteani, G., Steiger, R.H., 1989. Time calibration of a PT-path from the western Tauern Window, Eastern Alps: the problem of closure temperatures. Contributions to Mineralogy and Petrology 101, 1–11.

von Blanckenburg, F., Kagami, H., Deutsch, A., Oberli, F., Meier, M., Wiedenbeck, M., Barth, S., Fischer, H., 1998. The origin of Alpine plutons along the Periadriatic Lineament. Schweizerische Mineralogische und Petrographische Mitteilungen 78, 55–66.

Wilcox, R.E., Harding, T.P., Seely, D.R., 1973. Basic wrench tectonics. American Association of Petroleum Geologists Bulletin 57, 74–96.

Willemse, E.J.M., Pollard, D.D., 1998. On the orientation and patterns of wing cracks and solution surfaces at the tips of a sliding flaw or fault. Journal of Geophysical Research 103, 2427–2438.